

Supplementary Information for

# Overcoming Double-Step CO<sub>2</sub> Adsorption and Minimizing Water Co-Adsorption in Bulky Diamine-Appended Variants of Mg<sub>2</sub>(dobpdc)

Phillip J. Milner,<sup>a</sup> Jeffrey D. Martell,<sup>a</sup> Rebecca L. Siegelman,<sup>a</sup> David Gygi,<sup>b</sup> Simon C. Weston,<sup>c</sup>  
and Jeffrey R. Long<sup>a,d,e</sup>

<sup>a</sup>Department of Chemistry, University of California, Berkeley, CA 94720

<sup>b</sup>Department of Chemistry and Chemical Biology, Harvard University, Cambridge, MA, 02138

<sup>c</sup>Corporate Strategic Research, ExxonMobil Research and Engineering Company, Annandale, NJ 08801

<sup>d</sup>Department of Chemical Engineering, University of California, Berkeley, CA 94720

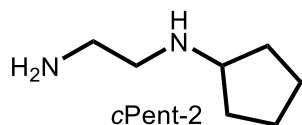
<sup>e</sup>Materials Sciences Division, Lawrence Berkeley National Lab, Berkeley, CA 94720

\* Correspondence to: jrlong@berkeley.edu

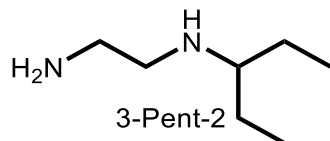
Table of contents	Page
1. Preparation of <i>primary,secondary</i> (1°,2°) diamines	S2
2. Synthesis of Mg <sub>2</sub> (dobpdc)	S5
3. <i>Primary,secondary</i> (1°,2°) diamines appended to Mg <sub>2</sub> (dobpdc)	S6
4. <i>Primary,tertiary</i> (1°,3°) diamines appended to Mg <sub>2</sub> (dobpdc)	S15
5. Preparation and characterization of Mg <sub>2</sub> (dotpdc)	S19
6. <i>Primary,secondary</i> (1°,2°) diamines appended to Mg <sub>2</sub> (dotpdc)	S23
7. <i>Primary,tertiary</i> (1°,3°) diamines appended to Mg <sub>2</sub> (dotpdc)	S31
8. Preparation and characterization of Mg <sub>2</sub> (pc-dobpdc)	S35
9. <i>Primary,secondary</i> (1°,2°) diamines appended to Mg <sub>2</sub> (pc-dobpdc)	S44
10. <i>Primary,tertiary</i> (1°,3°) diamines appended to Mg <sub>2</sub> (pc-dobpdc)	S52
11. Single-crystal X-ray diffraction structure of Zn <sub>2</sub> (pc-dobpdc)(DMA) <sub>2</sub>	S56
10. References	S58

## 1. Preparation of *primary,secondary* (1°,2°) diamines.

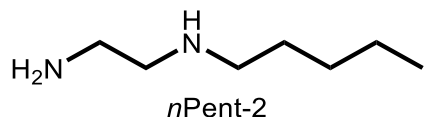
**General procedure for the synthesis of 1°,2°-alkylethylenediamines:** This procedure was adapted from the literature.<sup>1</sup> Ethylenediamine (30.0 equiv.) was added to a roundbottom flask equipped with a stir bar. The flask was cooled to 0 °C using an ice water bath. The alkyl halide (1.00 equiv.) was added dropwise over 10 min, and the reaction mixture was allowed to stir at room temperature for 1 h (in the case of primary alkyl halides) or 14 h (in the case of secondary alkyl halides). At this time, an equal volume of hexanes relative to ethylenediamine was added, and the reaction mixture was vigorously stirred for at least 4 h. The phases were separated, and the hexanes layer was washed with a small amount of brine to remove residual ethylenediamine. The hexanes layer was dried over MgSO<sub>4</sub> and filtered. The solvent was *carefully* removed with the aid of a rotary evaporator (Note: the water bath should be cooled to <10 °C to minimize evaporation of the diamine) to yield the desired diamine as a colorless oil. All diamines were found to be >95% pure as determined by both <sup>1</sup>H NMR and GC analysis, with the primary contaminant being residual ethylenediamine.



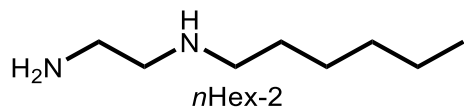
Following the general procedure, ethylenediamine (500 mL, 7.50 mol, 30.0 equiv.) and bromocyclopentane (26.8 mL, 250 mmol, 1.00 equiv.) were combined to yield *N*-(cyclopentyl)ethylenediamine (6.44 g, 20%) as a volatile colorless oil. <sup>1</sup>H NMR (400 MHz, CDCl<sub>3</sub>): δ 3.03 (pentet, *J* = 7 Hz, 1H), 2.77 (t, *J* = 6 Hz, 2H), 2.62 (t, *J* = 6 Hz, 2H), 1.76–1.86 (m, 2H), 1.59–1.70 (m, 2H), 1.44–1.55 (m, 2H), 1.22–1.33 (m, 2H), 1.16 (bs, 3H) ppm; <sup>13</sup>C NMR (100 MHz, CDCl<sub>3</sub>): δ 60.0, 51.6, 42.4, 33.5, 24.2 ppm. IR (neat): 3273, 2947, 2864, 1599, 1450, 1345, 1130, 1059, 793 cm<sup>-1</sup>. GC/MS calculated M<sup>+</sup> for C<sub>7</sub>H<sub>16</sub>N<sub>2</sub>: 128; found 128.



Following the general procedure, ethylenediamine (100 mL, 1.50 mol, 30.0 equiv.) and bromocyclopentane (6.21 mL, 50.0 mmol, 1.00 equiv.) were combined to yield *N*-(3-pentyl)ethylenediamine (3.44 g, 54%) as a volatile colorless oil.  $^1\text{H}$  NMR (300 MHz,  $\text{CDCl}_3$ ):  $\delta$  2.75 (t,  $J$  = 6 Hz, 2H), 2.60 (d,  $J$  = 6 Hz, 2H), 2.32 (pentet,  $J$  = 7 Hz, 1H), 1.39 (pentet,  $J$  = 7 Hz, 4H), 1.14 (bs, 3H), 0.85 (t,  $J$  = 7 Hz, 6H) ppm;  $^{13}\text{C}$  NMR (75 MHz,  $\text{CDCl}_3$ ):  $\delta$  60.1, 49.9, 42.5, 26.2, 10.1 ppm. IR (neat): 3301, 2960, 2932, 2873, 1583, 1460, 1380, 1154, 1103, 910, 707  $\text{cm}^{-1}$ .

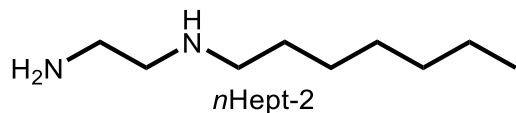


Following the general procedure, ethylenediamine (200 mL, 3.00 mol, 30.0 equiv.) and 1-bromopentane (12.4 mL, 100 mmol, 1.00 equiv.) were combined to yield *N*-(*n*-pentyl)ethylenediamine (4.72 g, 36%) as a volatile colorless oil.  $^1\text{H}$  NMR (400 MHz,  $\text{CDCl}_3$ ):  $\delta$  2.77 (t,  $J$  = 6 Hz, 2H), 2.63 (t,  $J$  = 6 Hz, 2H), 2.57 (t,  $J$  = 7 Hz, 2H), 1.41–1.50 (m, 2H), 1.24–1.32 (m, 4H), 1.18 (bs, 3H), 0.87 (t,  $J$  = 7 Hz, 3H) ppm;  $^{13}\text{C}$  NMR (100 MHz,  $\text{CDCl}_3$ ):  $\delta$  52.6, 49.8, 41.8, 29.8, 29.4, 22.5, 13.9 ppm. IR (neat): 3277, 2925, 2856, 2808, 1456, 1380, 1179, 1132, 1070, 845  $\text{cm}^{-1}$ . GC/MS calculated  $M^+$  for  $\text{C}_7\text{H}_{18}\text{N}_2$ : 130; found 130.



Following the general procedure, ethylenediamine (400 mL, 6.00 mol, 30.0 equiv.) and 1-bromohexane (28.0 mL, 200 mmol, 1.00 equiv.) were combined to yield *N*-(*n*-hexyl)ethylenediamine (14.4 g, 50%) as a volatile colorless oil.  $^1\text{H}$  NMR (400 MHz,  $\text{CDCl}_3$ ):  $\delta$  2.76 (t,  $J$  = 6 Hz, 2H), 2.62 (t,  $J$  = 6 Hz, 2H), 2.55 (t,  $J$  = 7 Hz, 2H), 1.44 (pentet,  $J$  = 7 Hz, 2H),

1.19–1.32 (m, 6H), 1.14 (bs, 3H), 0.84 (t,  $J = 7$  Hz, 3H) ppm;  $^{13}\text{C}$  NMR (100 MHz,  $\text{CDCl}_3$ ):  $\delta$  53.9, 50.2, 42.0, 32.0, 30.4, 27.2, 22.8, 14.2 ppm. IR (neat): 3297, 2924, 2854, 1522, 1457, 1377, 1131, 1077, 1033, 870, 827  $\text{cm}^{-1}$ . GC/MS calculated  $M^+$  for  $\text{C}_8\text{H}_{20}\text{N}_2$ : 144; found 144.



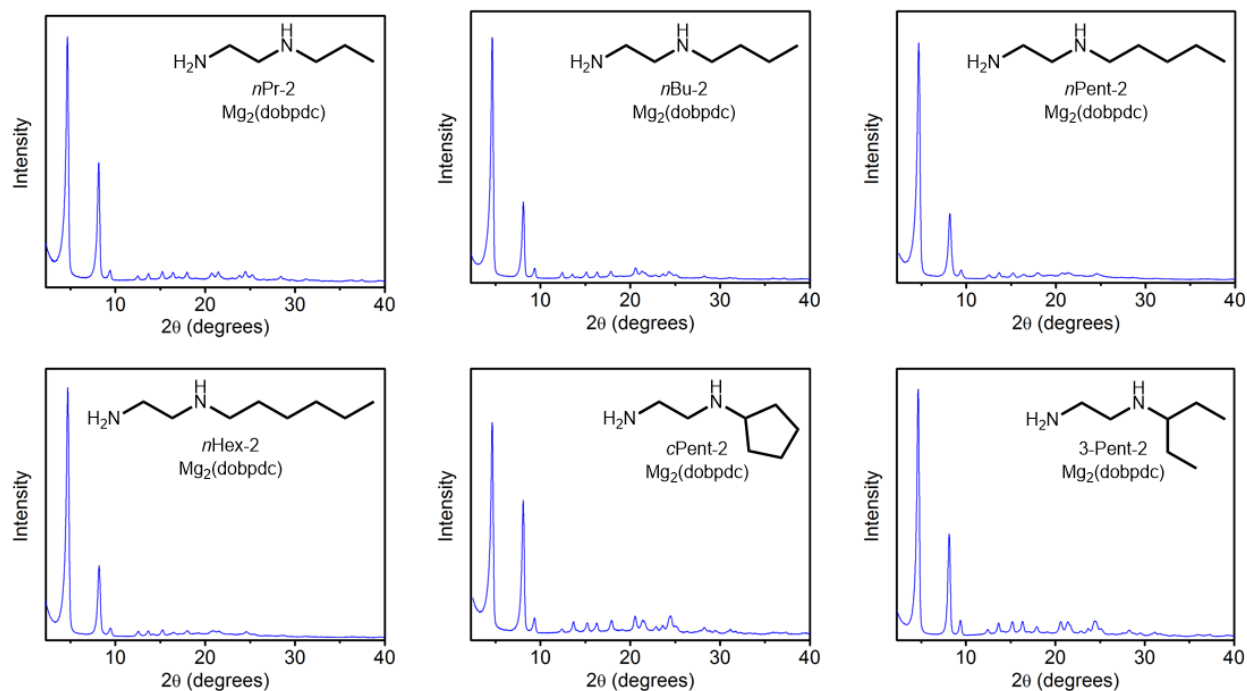
Following the general procedure, ethylenediamine (200 mL, ~3.00 mol, ~30 equiv.) and 1-bromoheptane (15.7 mL, 100 mmol, 1.00 equiv.) were combined to yield *N*-(*n*-heptyl)ethylenediamine (11.1 g, 70%) as a colorless oil.  $^1\text{H}$  NMR (400 MHz,  $\text{CDCl}_3$ ):  $\delta$  2.73 (t,  $J = 6$  Hz, 2H), 2.59 (t,  $J = 6$  Hz, 2H), 2.53 (t,  $J = 7$  Hz, 2H), 1.37–1.46 (m, 2H), 1.16–1.29 (m, 8H), 1.10 (bs, 3H), 0.81 (t,  $J = 7$  Hz, 3H) ppm;  $^{13}\text{C}$  NMR (100 MHz,  $\text{CDCl}_3$ ):  $\delta$  52.8, 50.1, 42.0, 31.9, 30.4, 29.4, 27.5, 22.7, 14.2 ppm. IR (neat): 3289, 2955, 2923, 2854, 1592, 1459, 1377, 1130, 822  $\text{cm}^{-1}$ . GC/MS calculated  $m/z$  for  $\text{C}_9\text{H}_{22}\text{N}_2$ : 158; found 158.

## 2. Synthesis of Mg<sub>2</sub>(dobpdc).

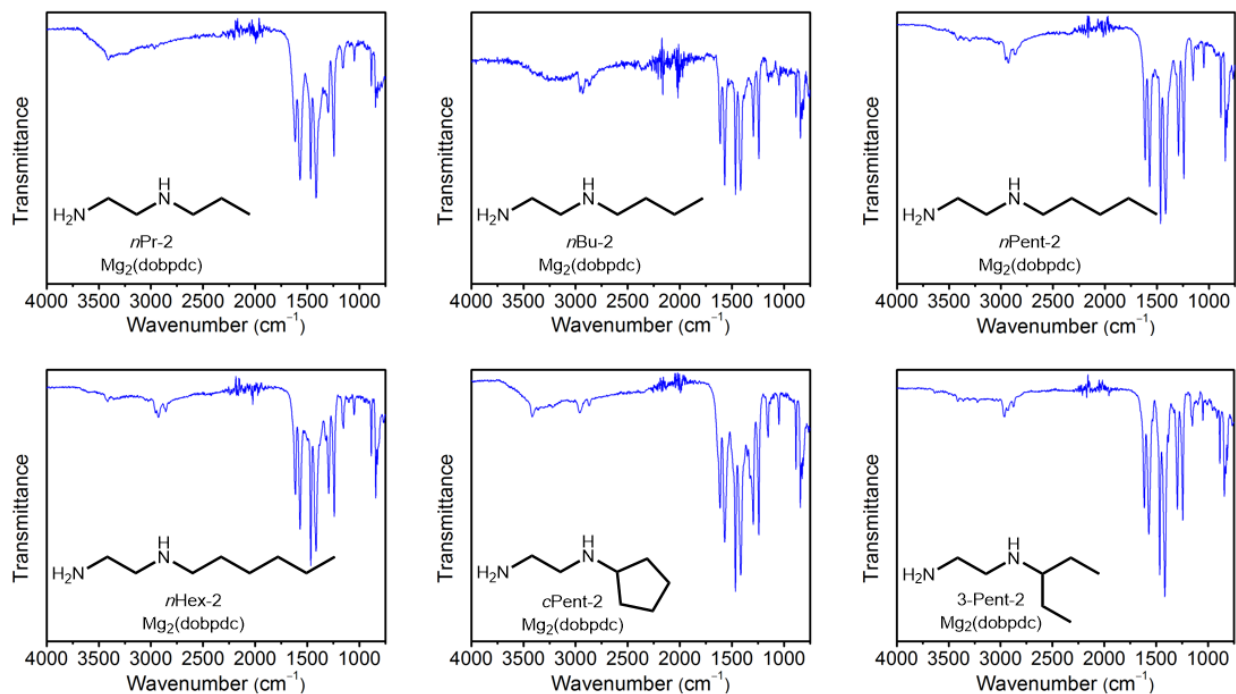
This procedure is adapted from the literature.<sup>2</sup> An Erlenmeyer flask was charged with Mg(NO<sub>3</sub>)<sub>2</sub>·6H<sub>2</sub>O (11.5 g, 45.0 mmol, 1.24 eq.), 4,4'-dihydroxy-[1,1'-biphenyl]-3,3'-dicarboxylic acid (9.90 g, 36.0 mmol, 1.00 eq.), *N,N*-dimethylformamide (90 mL), and methanol (110 mL). The mixture was sonicated until all of the solids dissolved. The mixture was filtered through filter paper into a 350 mL screw-cap high pressure reaction vessel equipped with a stir bar. The reaction mixture was sparged with N<sub>2</sub> for 1 h. The reaction vessel was sealed, and the reaction mixture was allowed to stir slowly at 120 °C for 14 h, resulting in precipitation of an off-white solid from solution. The non-homogenous mixture was filtered, and the solid was quickly transferred to a Pyrex jar filled with *N,N*-dimethylformamide (500 mL). The jar was placed in an oven heated to 60 °C and allowed to stand for at least 3 h. At this time, the jar was cooled to room temperature, the solvent was decanted and replaced with fresh *N,N*-dimethylformamide (500 mL), and the jar was placed in an oven heated to 60 °C. This washing process was repeated a total of three times. The *N,N*-dimethylformamide was replaced with methanol (500 mL), and the jar was placed in an oven heated to 60 °C and allowed to stand for at least 3 h. At this time, the jar was cooled to room temperature, the solvent was decanted and replaced with fresh methanol (500 mL), and the jar was placed in an oven heated to 60 °C. This washing process was repeated a total of three times. A small portion of the solid was removed and placed in a vial under flowing N<sub>2</sub>. The solid was activated under flowing N<sub>2</sub> at 180 °C for 24 h, transferred to an ASAP tube, and activated for an additional 24 h under reduced pressure (<10 μbar) at 180 °C. Activated Mg<sub>2</sub>(dobpdc) was obtained as an off-white solid. Langmuir surface area determined from the 77 K N<sub>2</sub> adsorption isotherm: 3780 m<sup>2</sup>/g.

### 3. *Primary,secondary* (1°,2°) diamines appended to Mg<sub>2</sub>(dobpdc).

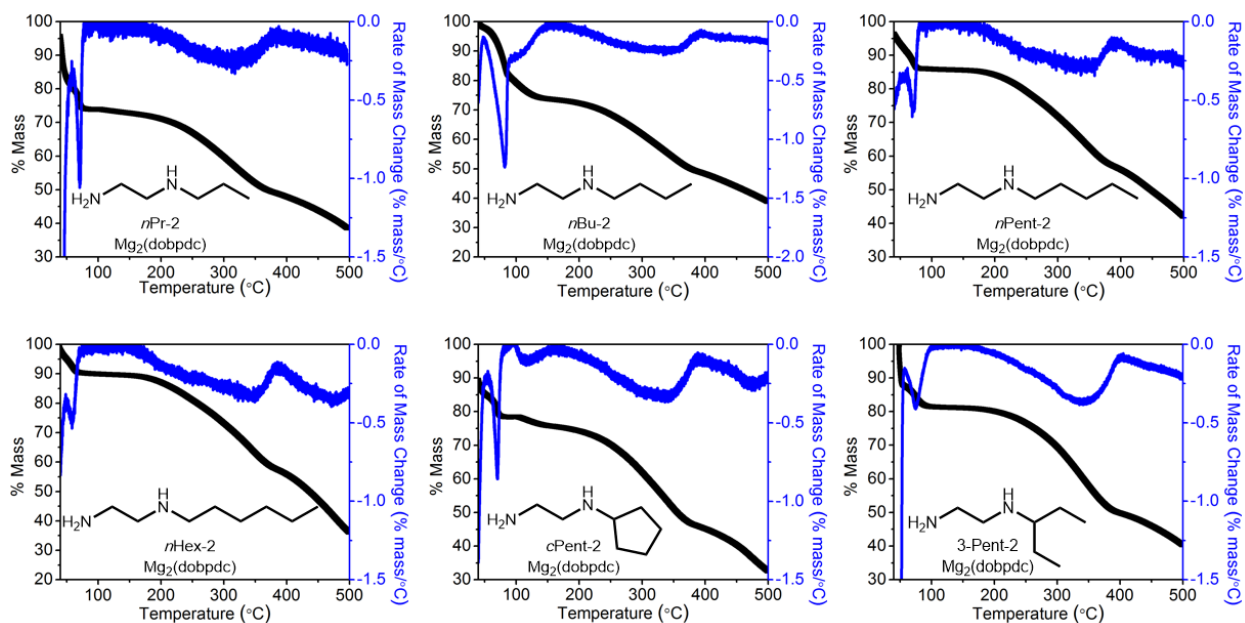
The preparations of e-2-Mg<sub>2</sub>(dobpdc) and i-2-Mg<sub>2</sub>(dobpdc) have been previously reported.<sup>2</sup> The other diamine-appended variants of Mg<sub>2</sub>(dobpdc) in this section were prepared according to the procedure outlined in the Experimental section. All attempts to prepare *n*Hept-2-Mg<sub>2</sub>(dobpdc) yielded materials with low diamine loadings (~69%) that did not display step-shaped adsorption of CO<sub>2</sub>.



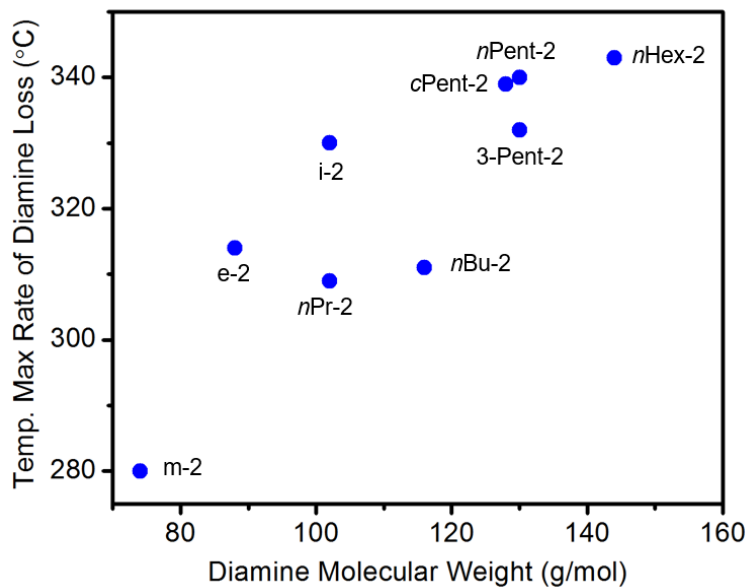
**Figure S1.** Powder X-ray diffraction patterns (CuKα radiation,  $\lambda = 1.5418 \text{ \AA}$ ) of as-synthesized samples of 1°,2°-alkylethylenediamine-appended variants of Mg<sub>2</sub>(dobpdc).



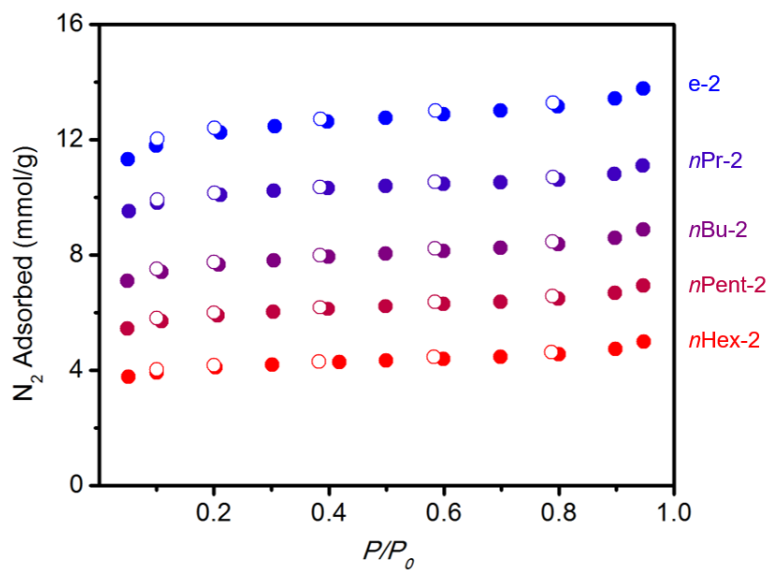
**Figure S2.** IR spectra of as-synthesized samples of 1°,2°-alkylethylenediamine-appended variants of Mg<sub>2</sub>(dobpdc).



**Figure S3.** Dry N<sub>2</sub> decomposition profiles of 1°,2°-alkylethylenediamine-appended variants of Mg<sub>2</sub>(dobpdc). The rate of mass change at each temperature is shown in blue. A ramp rate of 1.5 °C/min was used.

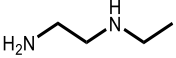
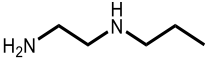
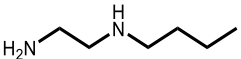
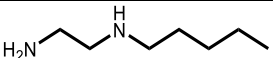
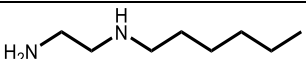
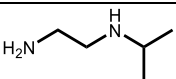
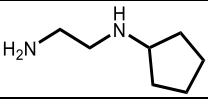
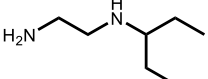


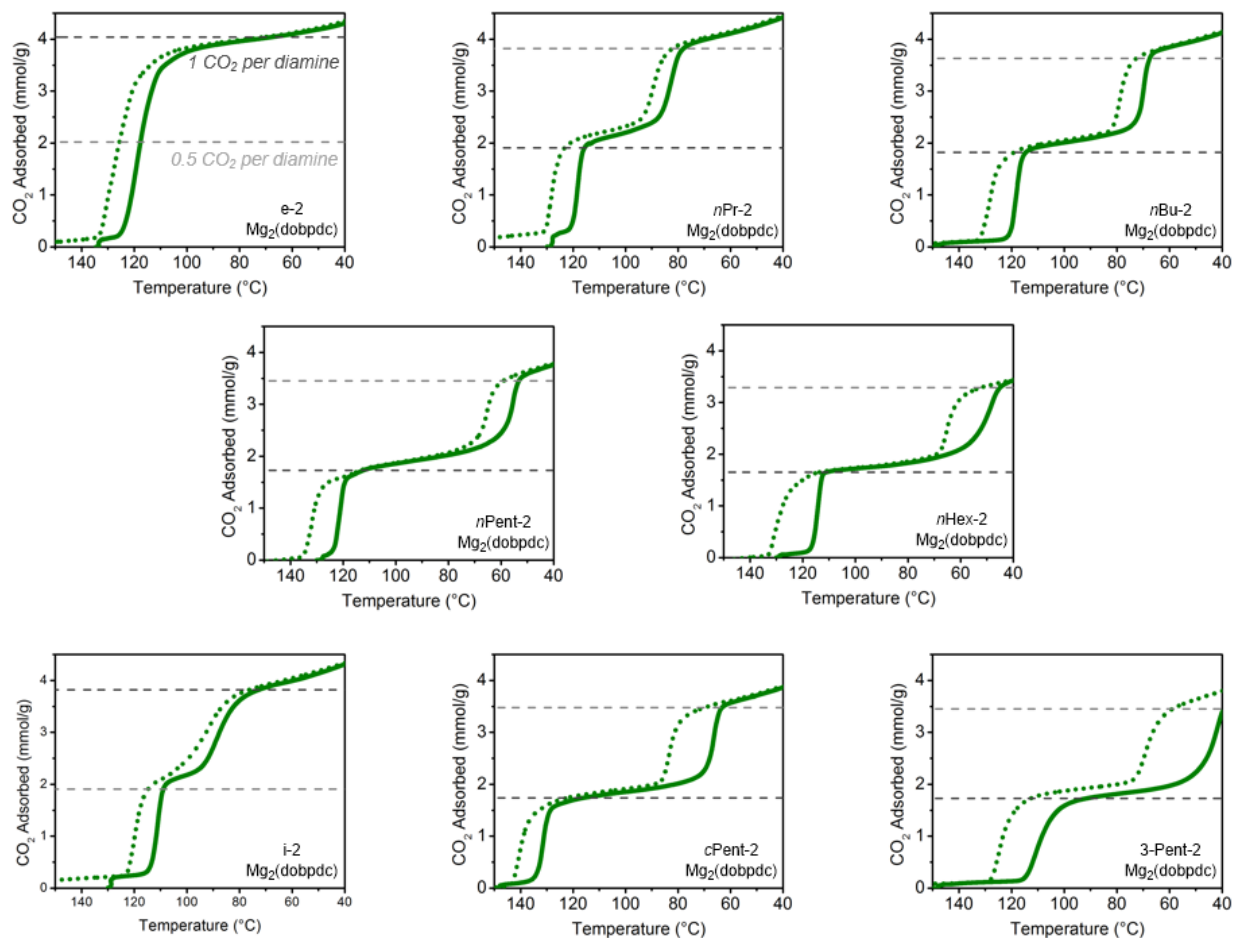
**Figure S4.** Temperature of the maximum rate of diamine loss (determined from the plots in Figure S3) vs. diamine molecular weight for 1°,2°-alkylethylenediamine-appended variants of  $\text{Mg}_2(\text{dobpdc})$ . This plot confirms that increasing the molecular weight of the diamine makes the adsorbent less susceptible to diamine loss. The data for m-2, e-2, and i-2 are taken from the literature with permission.<sup>2</sup>



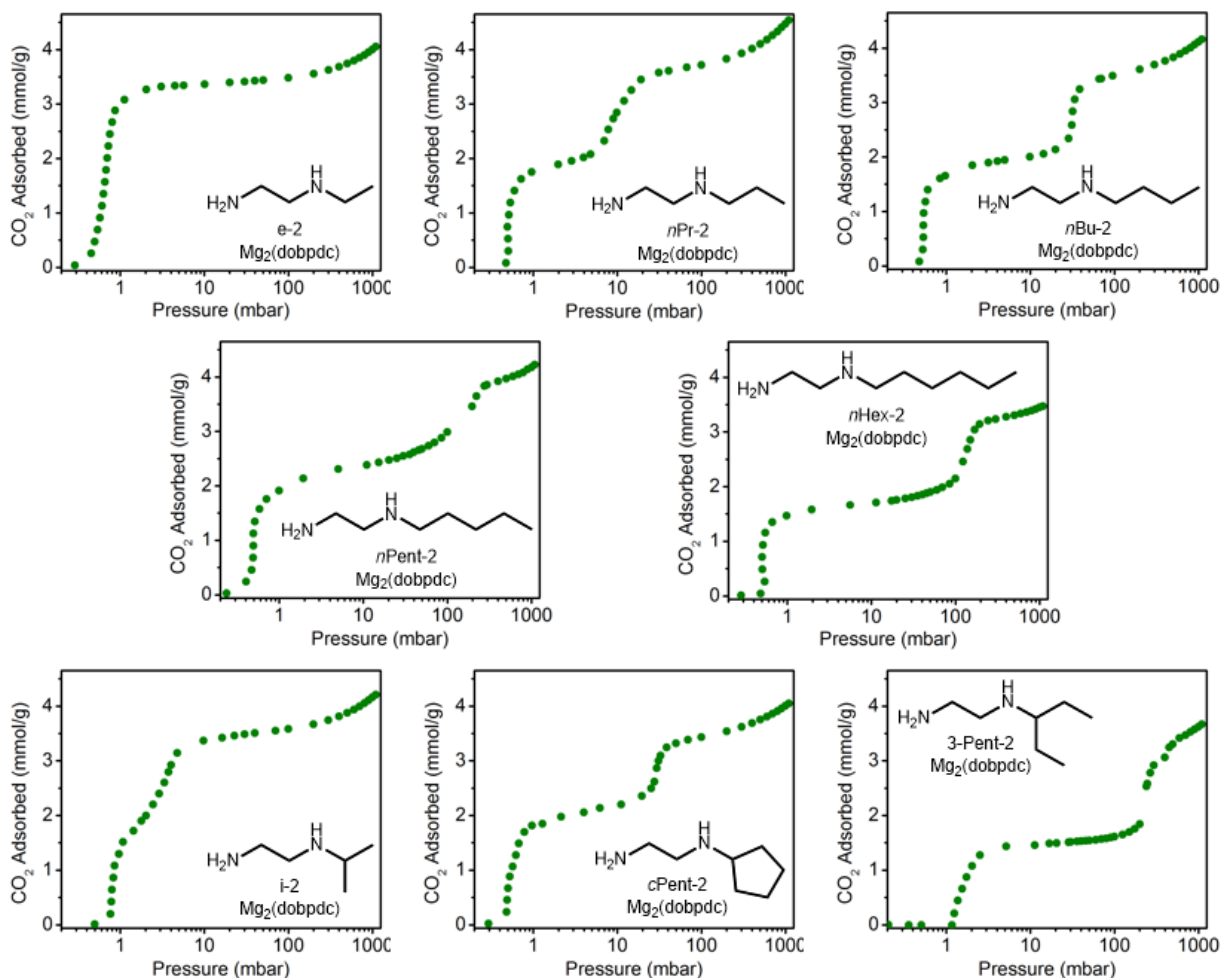
**Figure S5.** 77K  $\text{N}_2$  adsorption isotherms of activated e-2-, nPr-2-, nBu-2-, nPent-2-, and nHex-2- $\text{Mg}_2(\text{dobpdc})$ . The Langmuir surface areas from these adsorption isotherms were determined to be 1370, 1090, 892, 698, and 503  $\text{m}^2/\text{g}$ , respectively. After these isotherms, the adsorbents were digested to confirm both the absence of toluene and high diamine loadings (e-2: 100%; nPr-2: 100%; nBu-2: 101%; nPent-2: 93%; nHex-2: 92%) in every case.

**Table S1.** Typical diamine loadings and activation temperatures of 1°,2°-alkylethylenediamine-appended variants of Mg<sub>2</sub>(dobpdc).

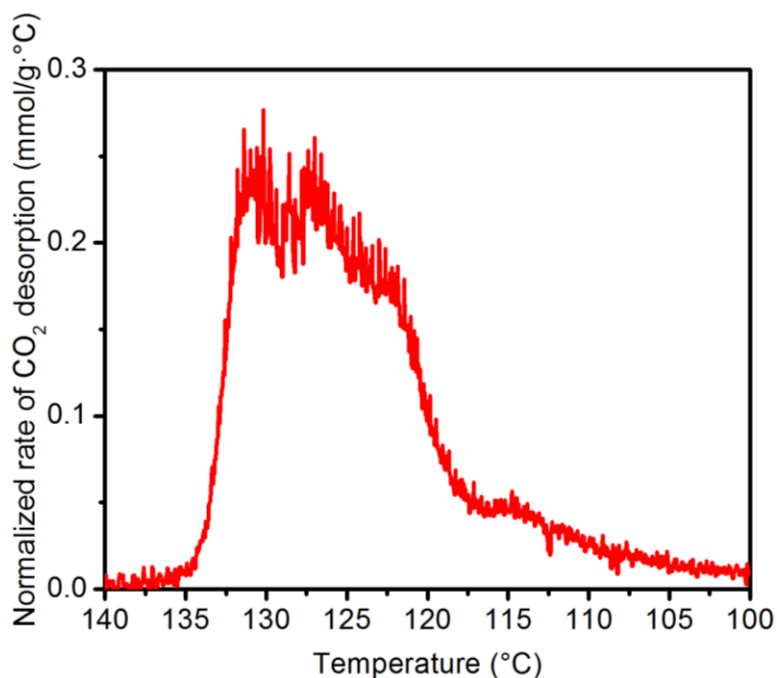
Diamine	Diamine loading as synthesized	Activation temp. (°C)	Diamine loading after humid N <sub>2</sub> activation
	103% <sup>2</sup>	130	97%
	104%	130	95%
	107%	150	95%
	96%	130	97%
	90%	130	89%
	102% <sup>2</sup>	130	100%
	103%	150	99%
	93%	130	92%



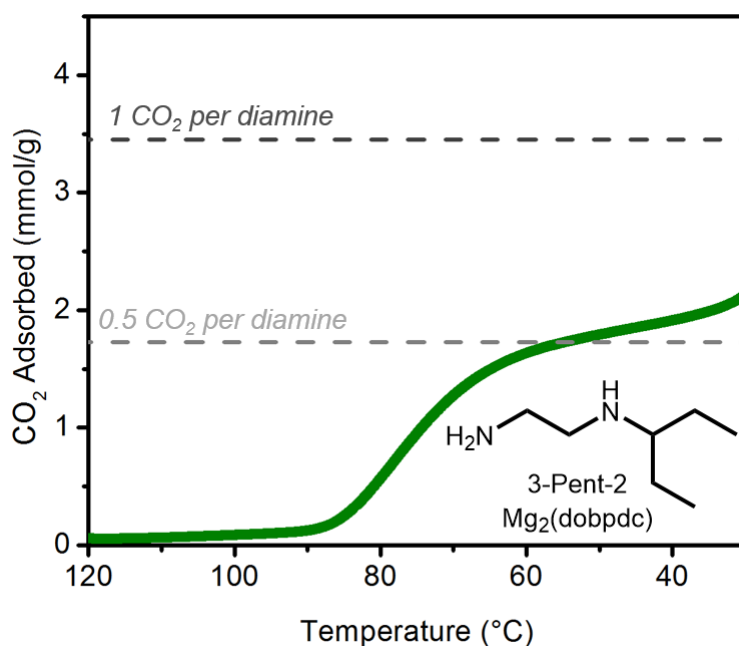
**Figure S6.** Pure CO<sub>2</sub> adsorption (solid) and desorption (dotted) isobars for a series of 1°,2°-alkylethylenediamine-appended variants of Mg<sub>2</sub>(dobpdc). The CO<sub>2</sub> capacities assuming the adsorption of one CO<sub>2</sub> per diamine (dark gray dashed lines) and 0.5 CO<sub>2</sub> per diamine (light gray dashed lines) are indicated in each case. A ramp rate of 2 °C/min was used.



**Figure S7.** 40 °C CO<sub>2</sub> isotherms of 1°,2°-alkylethylenediamine-appended variants of Mg<sub>2</sub>(dobpdc). The pressure at which the second CO<sub>2</sub> adsorption step occurs follows the same trend as observed in isobaric measurements, with larger alkyl substituents leading to higher adsorption step pressures.

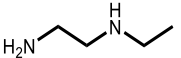
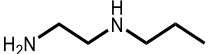
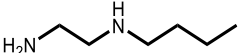
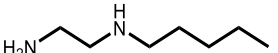
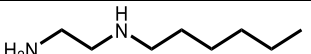
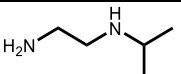
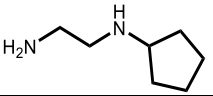
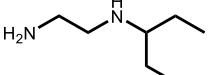


**Figure S8.** Temperature derivative of the pure CO<sub>2</sub> desorption isobar of e-2-Mg<sub>2</sub>(dobpdc) showing the possible presence of two close CO<sub>2</sub> desorption steps. A ramp rate of 1 °C/min was used.

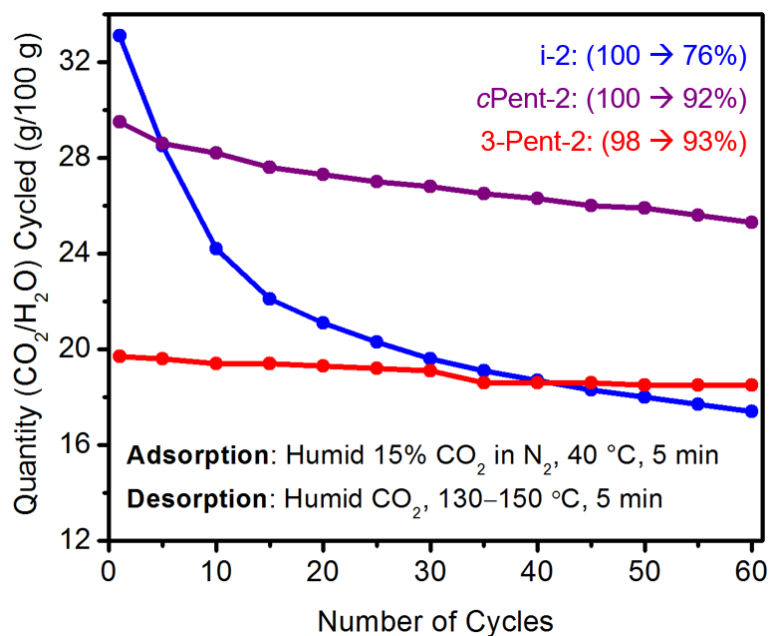


**Figure S9.** Dry 15% CO<sub>2</sub> in N<sub>2</sub> adsorption isobar of 3-Pent-2-Mg<sub>2</sub>(dobpdc), revealing that the second CO<sub>2</sub> adsorption step is not operative under this gas stream at temperatures above 30 °C, leading to half the expected capacity for CO<sub>2</sub>. A ramp rate of 2 °C/min was used.

**Table S2.** Dry CO<sub>2</sub>, humid N<sub>2</sub>, and humid CO<sub>2</sub> capacities and estimated amounts of water co-adsorption for 1°,2°-alkylethylenediamine-appended variants of Mg<sub>2</sub>(dobpdc) at 40 °C, determined from isobaric cooling measurements (see Figures 3-4 in the main text).

Diamine	Dry CO <sub>2</sub> uptake (g/100 g)	Humid N <sub>2</sub> uptake (g/100 g)	Humid CO <sub>2</sub> uptake (g/100 g)	Estimated water co-adsorption (g/ 100 g)	Estimated water co-adsorption (per diamine)
	19.2	8.4	20.7	1.5	0.2
	19.5	7.0	22.7 <sup>a</sup>	3.2	0.5
	18.2	7.2	21.2 <sup>a</sup>	3.0	0.5
	17.0	6.3	19.7	2.7	0.4
	15.4	5.7	18.2	2.8	0.5
	18.1	6.1	21.4	3.3	0.5
	17	6.1	22.4 <sup>a</sup>	5.4	0.9
	14.9	2.2	19.8	4.9	0.8

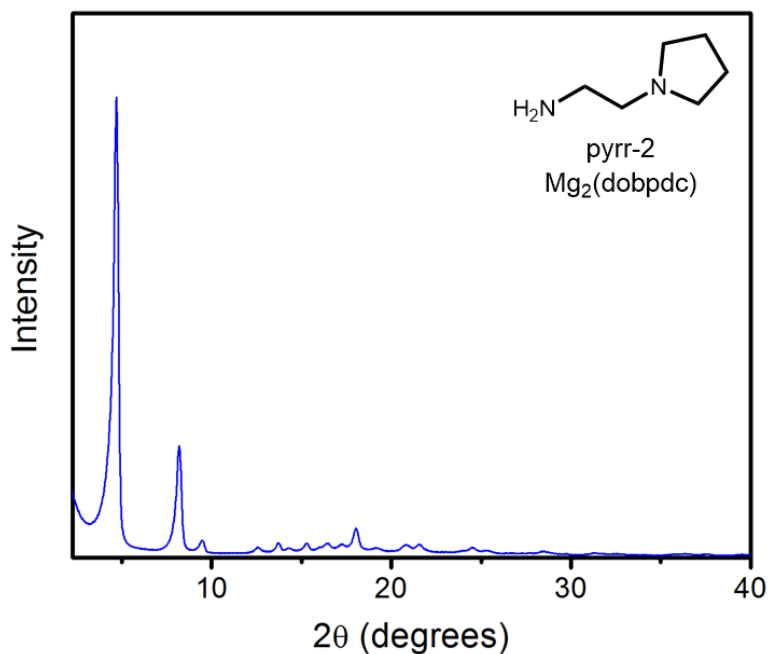
<sup>a</sup>In these cases, increased water co-adsorption was observed upon holding the adsorbent at 40 °C under flowing wet CO<sub>2</sub>, suggesting that the values listed above are not equilibrium values and thus represent only lower bounds for the extent of water co-adsorption. In all other cases, minimal additional uptake was observed upon holding the adsorbents at 40 °C under flowing humid pure CO<sub>2</sub>.



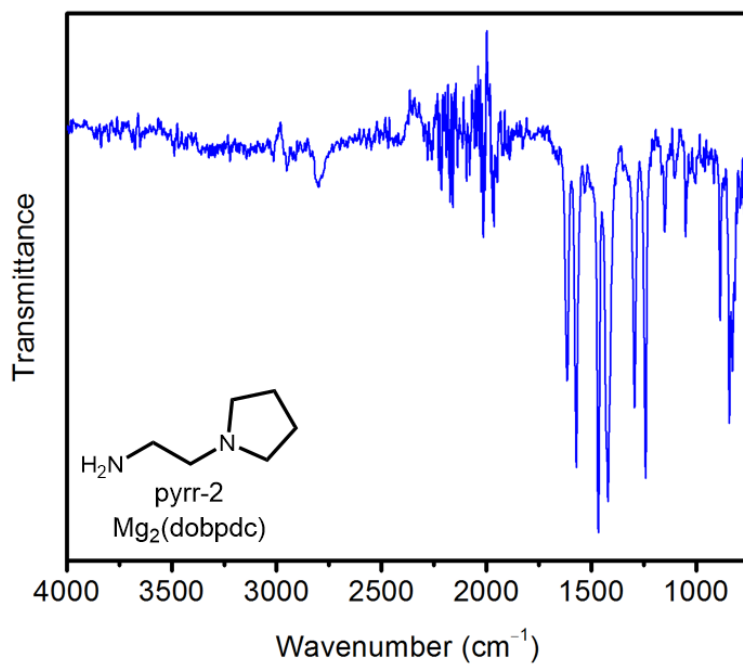
**Figure S10.** Cycling stability of branched 1°,2°-alkylethylenediamine-appended variants of  $\text{Mg}_2(\text{dobpdc})$  in a simulated temperature swing adsorption process. The diamine loadings before and after 60 cycles are indicated in each case in the upper right corner.

#### 4. *Primary, tertiary* ( $1^\circ, 3^\circ$ ) diamines appended to $\text{Mg}_2(\text{dobpdc})$ .

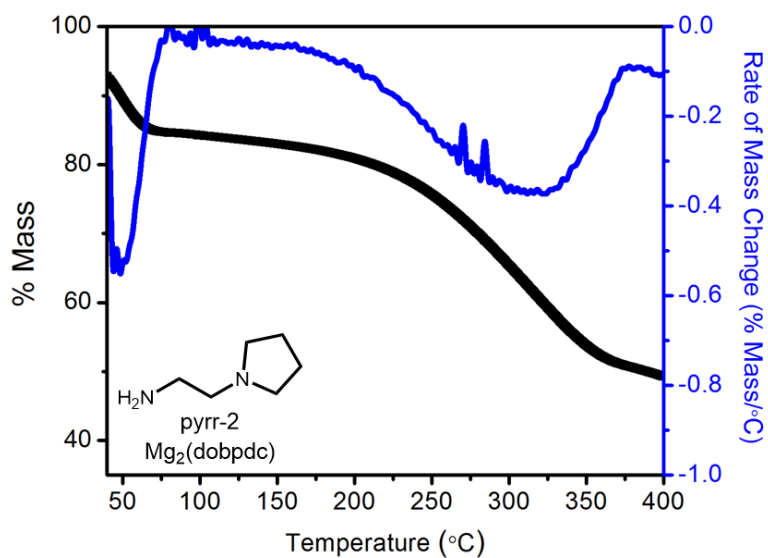
The preparation of ee-2- $\text{Mg}_2(\text{dobpdc})$  has been previously reported.<sup>2</sup> The framework pyrr-2- $\text{Mg}_2(\text{dobpdc})$  was prepared according to the procedure outlined in the Experimental section.



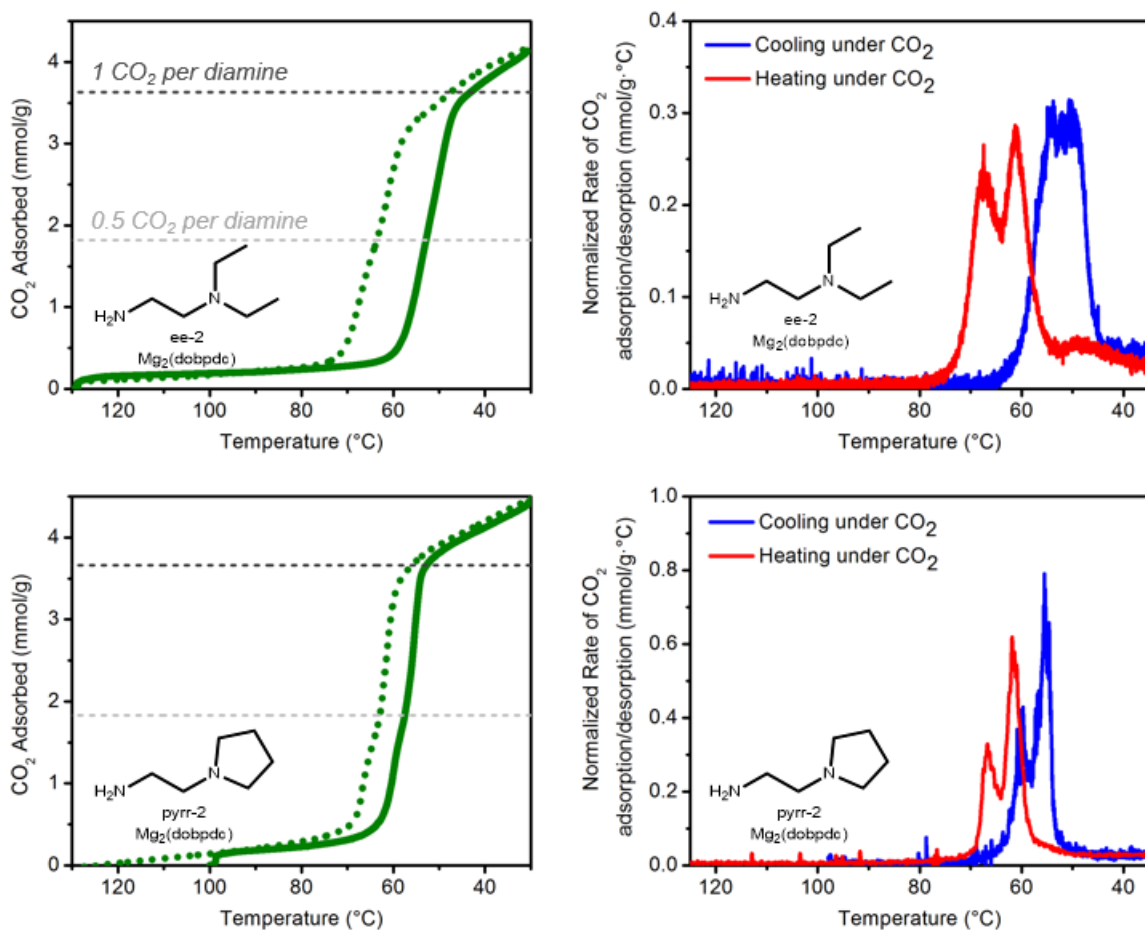
**Figure S11.** Powder X-ray diffraction pattern ( $\text{CuK}\alpha$  radiation,  $\lambda = 1.5418 \text{ \AA}$ ) of as-synthesized pyrr-2- $\text{Mg}_2(\text{dobpdc})$ . The diamine loading of this sample was found to be 99%, as determined by  $^1\text{H}$  NMR after digestion with  $\text{DCl}$ .<sup>2</sup>



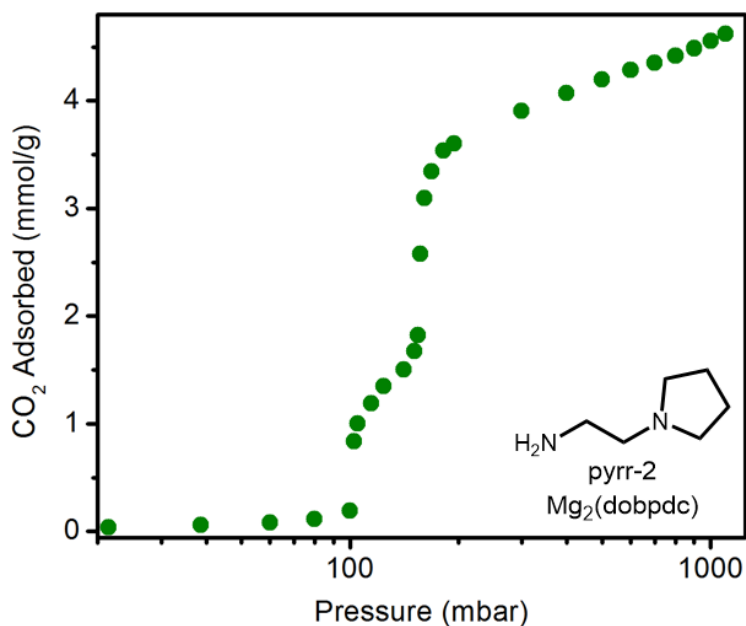
**Figure S12.** IR spectrum of as-synthesized pyrr-2–Mg<sub>2</sub>(dobpdc).



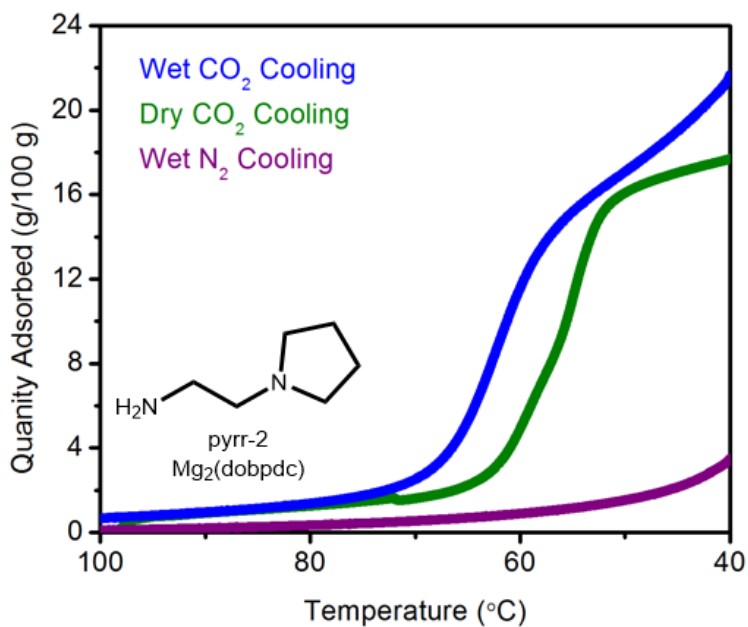
**Figure S13.** Dry N<sub>2</sub> decomposition profile of pyrr-2–Mg<sub>2</sub>(dobpdc). The rate of mass change at each temperature is shown in blue. A ramp rate of 1.5 °C/min was used.



**Figure S14.** Left: CO<sub>2</sub> adsorption (solid line) and desorption (dotted line) isobars for Mg<sub>2</sub>(dobpdc) appended with ee-2 (top) and pyr-2 (bottom). Right: The derivative plots of these isobars show two CO<sub>2</sub> adsorption (blue) and desorption (red) steps. The data for ee-2–Mg<sub>2</sub>(dobpdc) is reproduced from the literature with permission.<sup>2</sup> A ramp rate of 2 °C/min was used.



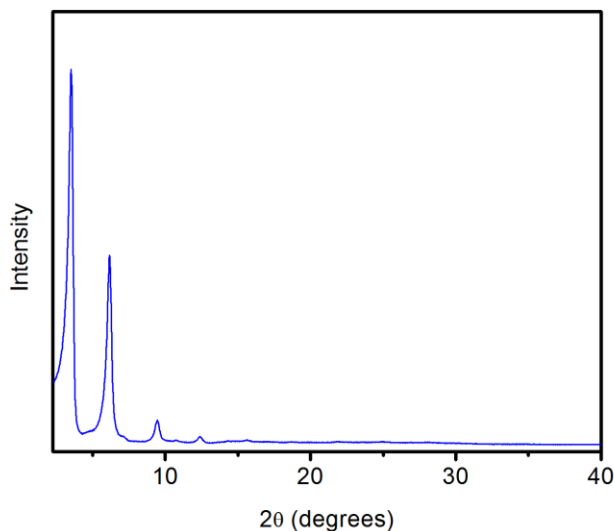
**Figure S15.** 40 °C CO<sub>2</sub> isotherm of pyr-2-Mg<sub>2</sub>(dobpdc), showing two distinct adsorption steps. Previously reported isotherms of ee-2-Mg<sub>2</sub>(dobpdc) also showed the presence of two adsorption steps.<sup>2</sup>



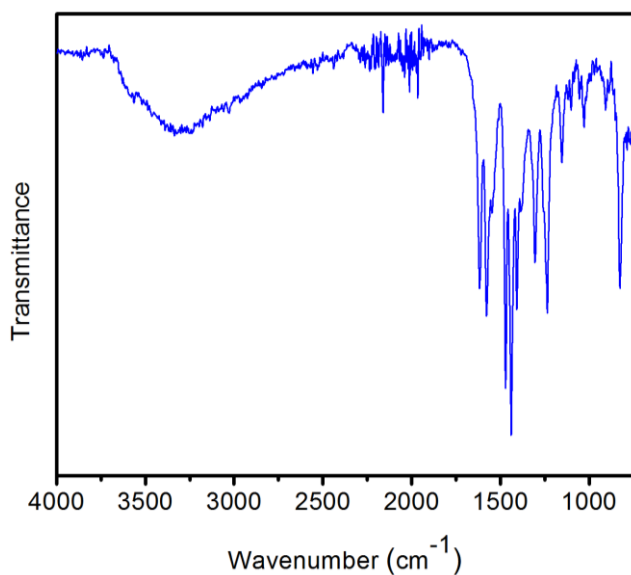
**Figure S16.** Humid N<sub>2</sub> (purple), dry CO<sub>2</sub> (green), and humid CO<sub>2</sub> (blue) adsorption isobars of pyr-2-Mg<sub>2</sub>(dobpdc). The apparent CO<sub>2</sub> adsorption steps are shifted to higher temperatures under humid conditions, accompanied by significant water co-adsorption. The diamine loading was found to be 99% after the humid TGA experiments, as determined by <sup>1</sup>H NMR after digestion with DCl. A ramp rate of 2 °C/min was used.

## 5. Preparation and characterization of $\text{Mg}_2(\text{dotpdc})$ .

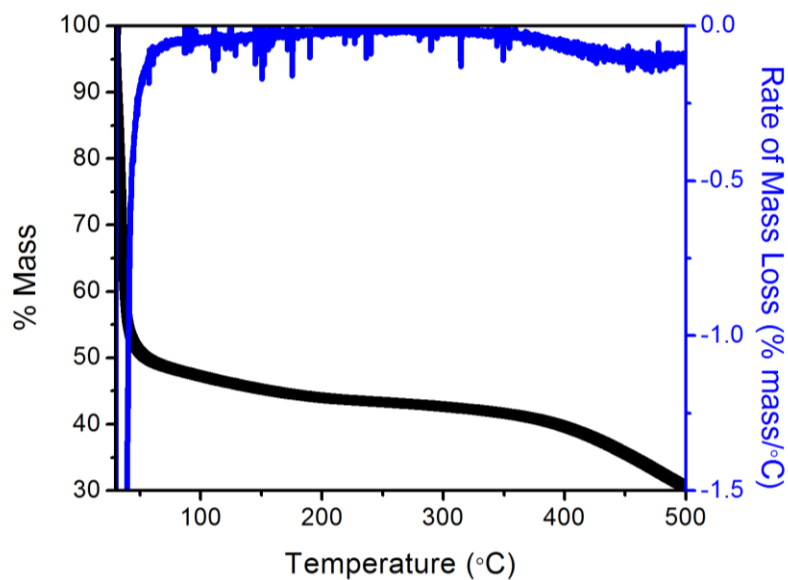
$\text{Mg}_2(\text{dotpdc})$  was prepared according to the procedure outlined in the Experimental section. Large scale batches of  $\text{Mg}_2(\text{dotpdc})$  were prepared by combining the product from multiple 20 mL scintillation vials prior to washing.



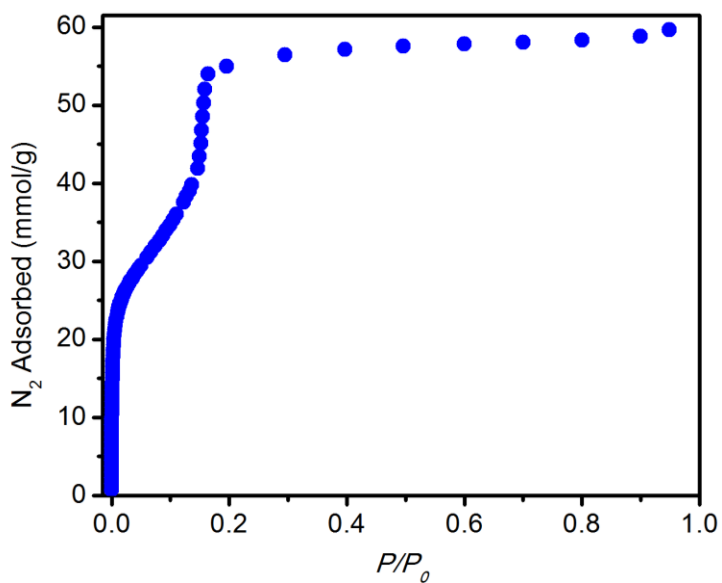
**Figure S17.** Powder X-ray diffraction pattern ( $\text{CuK}\alpha$  radiation,  $\lambda = 1.5418 \text{ \AA}$ ) of MeOH-solvated  $\text{Mg}_2(\text{dotpdc})$ .



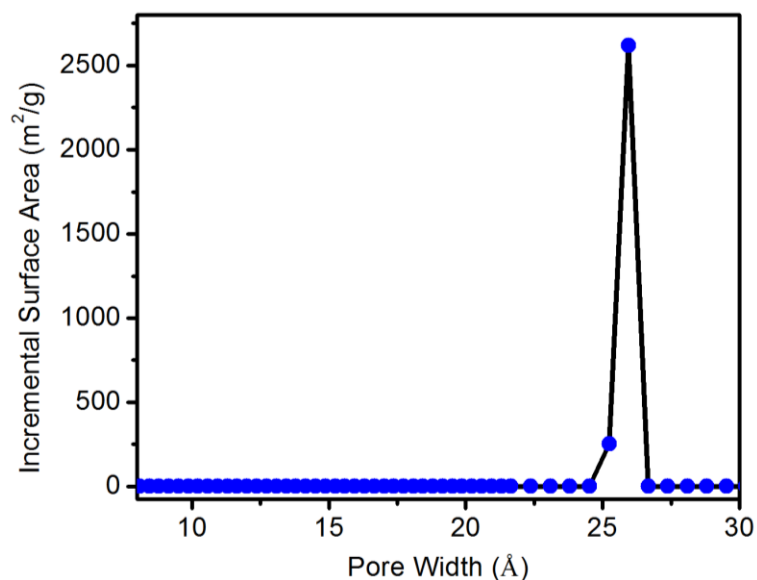
**Figure S18.** IR spectrum of MeOH-solvated  $\text{Mg}_2(\text{dotpdc})$ , confirming that washing with MeOH is sufficient to remove *N,N*-dimethylformamide from the open  $\text{Mg}^{2+}$  sites.



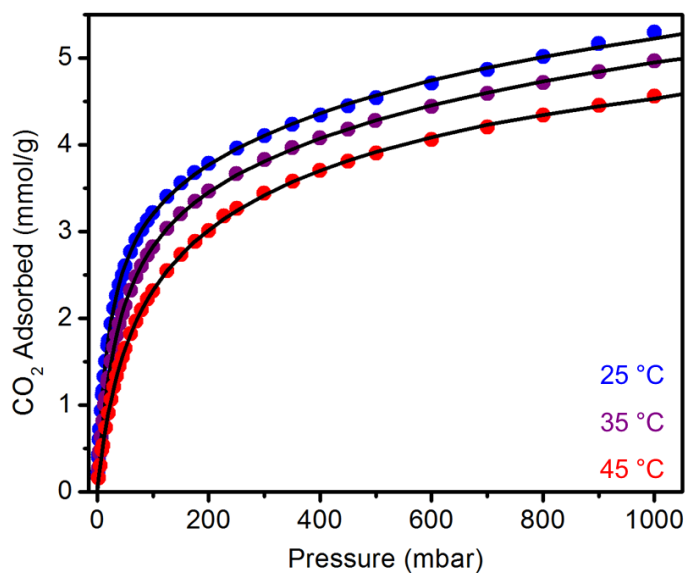
**Figure S19.** Dry N<sub>2</sub> decomposition profile of MeOH-solvated Mg<sub>2</sub>(dotpdc). The rate of mass change at each temperature is shown in blue. The framework is stable until approximately 350 °C. A ramp rate of 1.5 °C/min was used.



**Figure S20.** 77K N<sub>2</sub> adsorption isotherm of activated Mg<sub>2</sub>(dotpdc). Fitting these data yielded a Brunauer–Emmett–Teller surface area of  $3100 \pm 30 \text{ m}^2/\text{g}$  and a Langmuir surface area of  $5840 \pm 30 \text{ m}^2/\text{g}$ .



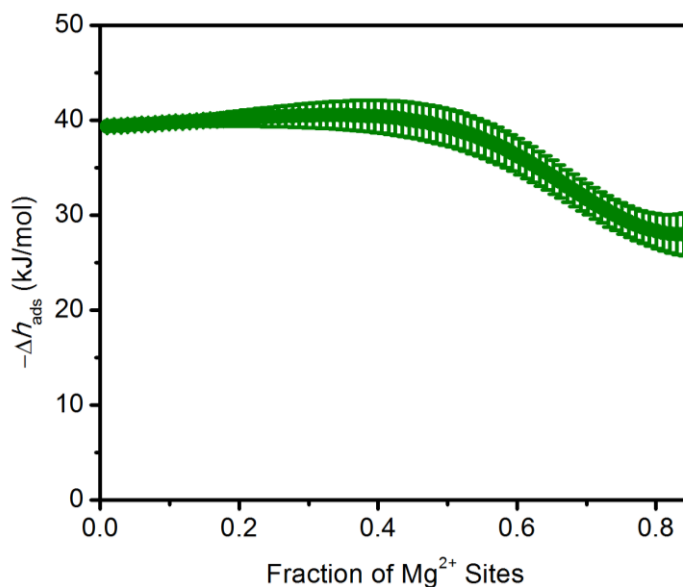
**Figure S21.** DFT pore size distribution of activated  $\text{Mg}_2(\text{dotpdc})$  calculated from the 77K  $\text{N}_2$  adsorption isotherm (Figure S20) assuming a metal oxide surface with a cylinder pore geometry. The pores are estimated to be 26 Å in diameter, which is consistent with the pore diameter determined previously for the Fe analogue.<sup>3</sup>



**Figure S22.** 25 (blue), 35 (purple), and 45 °C (red)  $\text{CO}_2$  isotherms of activated  $\text{Mg}_2(\text{dotpdc})$ . Independently fit dual-site Langmuir-Freundlich models are shown.

**Table S3.** Dual-site Langmuir-Freundlich parameters for the independently fit CO<sub>2</sub> isotherms of Mg<sub>2</sub>(dotpdc) at 25, 35, and 45 °C.

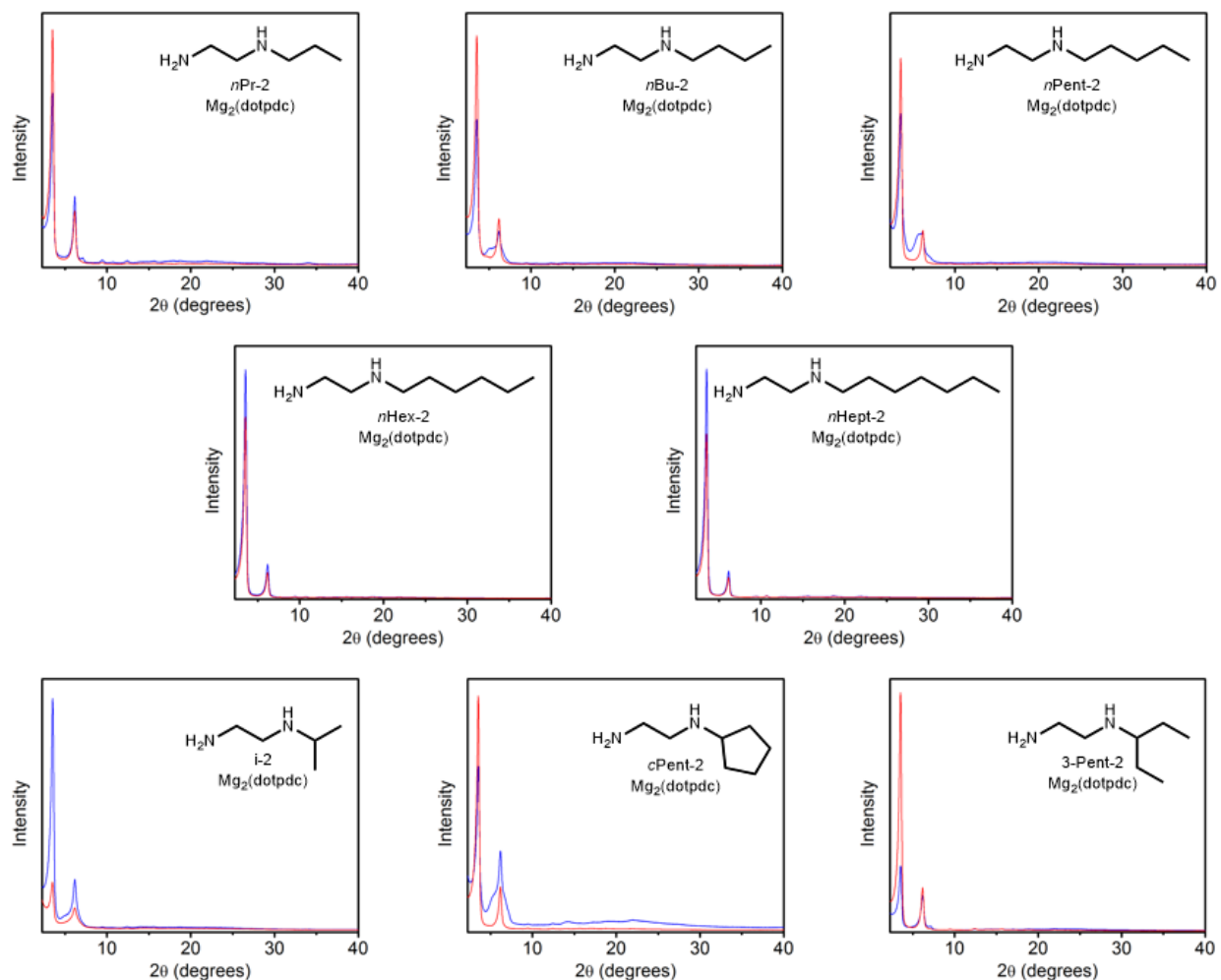
Parameter	25 °C	35 °C	45 °C
$q_{sat1}$ (mmol/g)	3.47	3.47	2.88
$b_1$ (bar <sup>-1</sup> )	47.1	28.0	19.8
$v_1$	1	1	1
$q_{sat2}$ (mmol/g)	3.47	3.40	2.85
$b_2$ (bar <sup>-1</sup> )	1.12	0.89	1.69
$v_2$	1	1	1



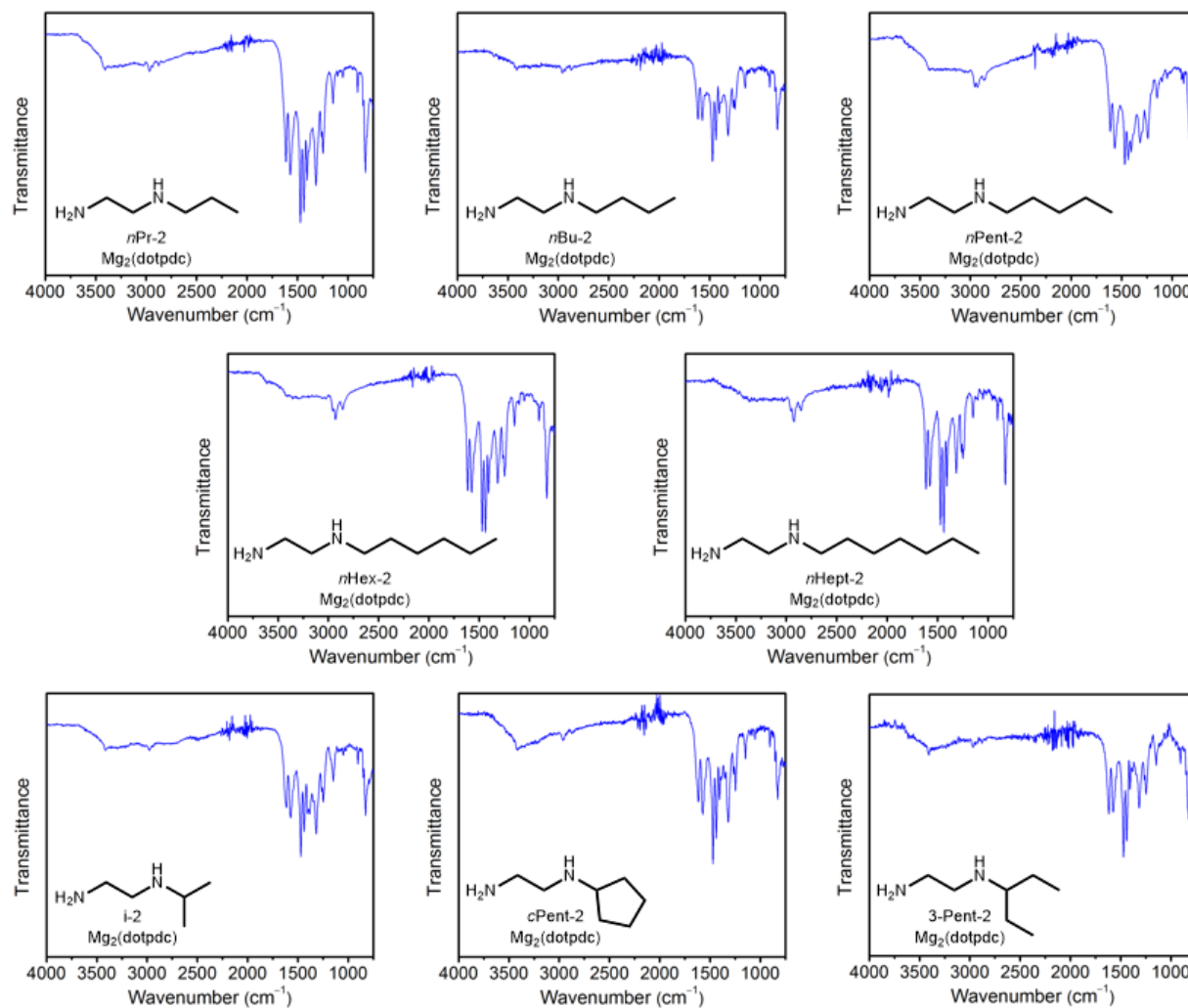
**Figure S23.** CO<sub>2</sub> differential heats of adsorption as a function of fraction of occupied metal sites in activated Mg<sub>2</sub>(dotpdc). The differential heat of adsorption at low loadings (~40 kJ/mol) is similar to that previously reported for Mg<sub>2</sub>(dobpdc) (~43 kJ/mol).<sup>4</sup>

## 6. Primary,secondary (1°,2°) diamines appended to Mg<sub>2</sub>(dotpdc).

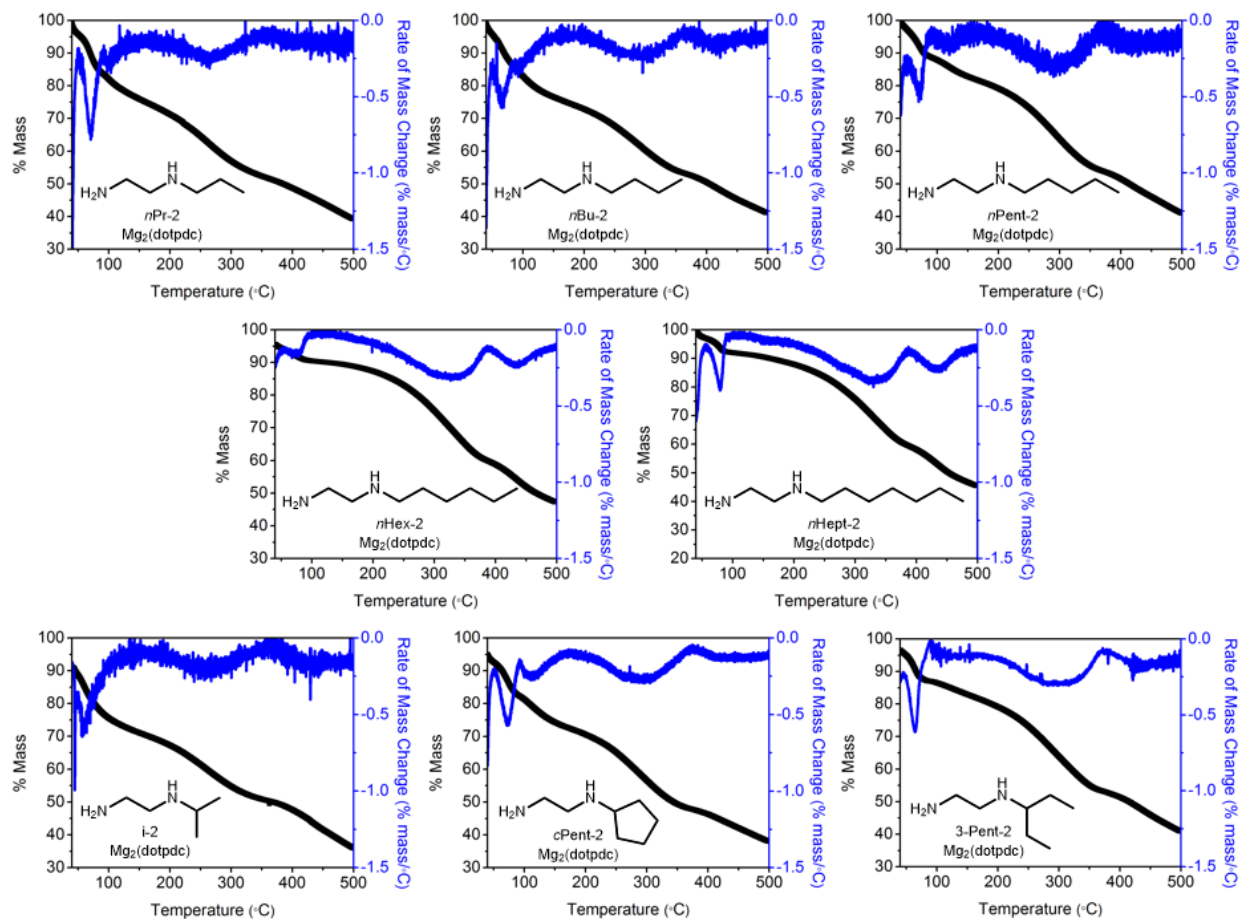
Diamine-appended variants of Mg<sub>2</sub>(dotpdc) were prepared following the procedure in the Experimental section. All attempts to date to prepare e-2-Mg<sub>2</sub>(dotpdc) have yielded inconsistent results due to the seemingly poor stability of Mg<sub>2</sub>(dotpdc) to exposure to e-2.



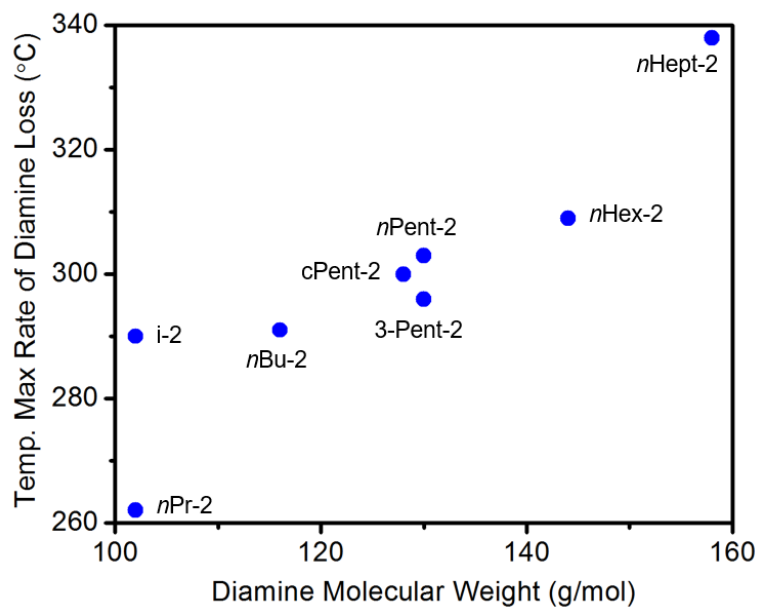
**Figure S24.** Powder X-ray diffraction patterns (CuK $\alpha$  radiation,  $\lambda = 1.5418 \text{ \AA}$ ) of as-synthesized (blue) and activated (red) samples of 1°,2°-alkylethylenediamine-appended variants of Mg<sub>2</sub>(dotpdc). The activated patterns demonstrate that this adsorbents remain crystalline upon activation.



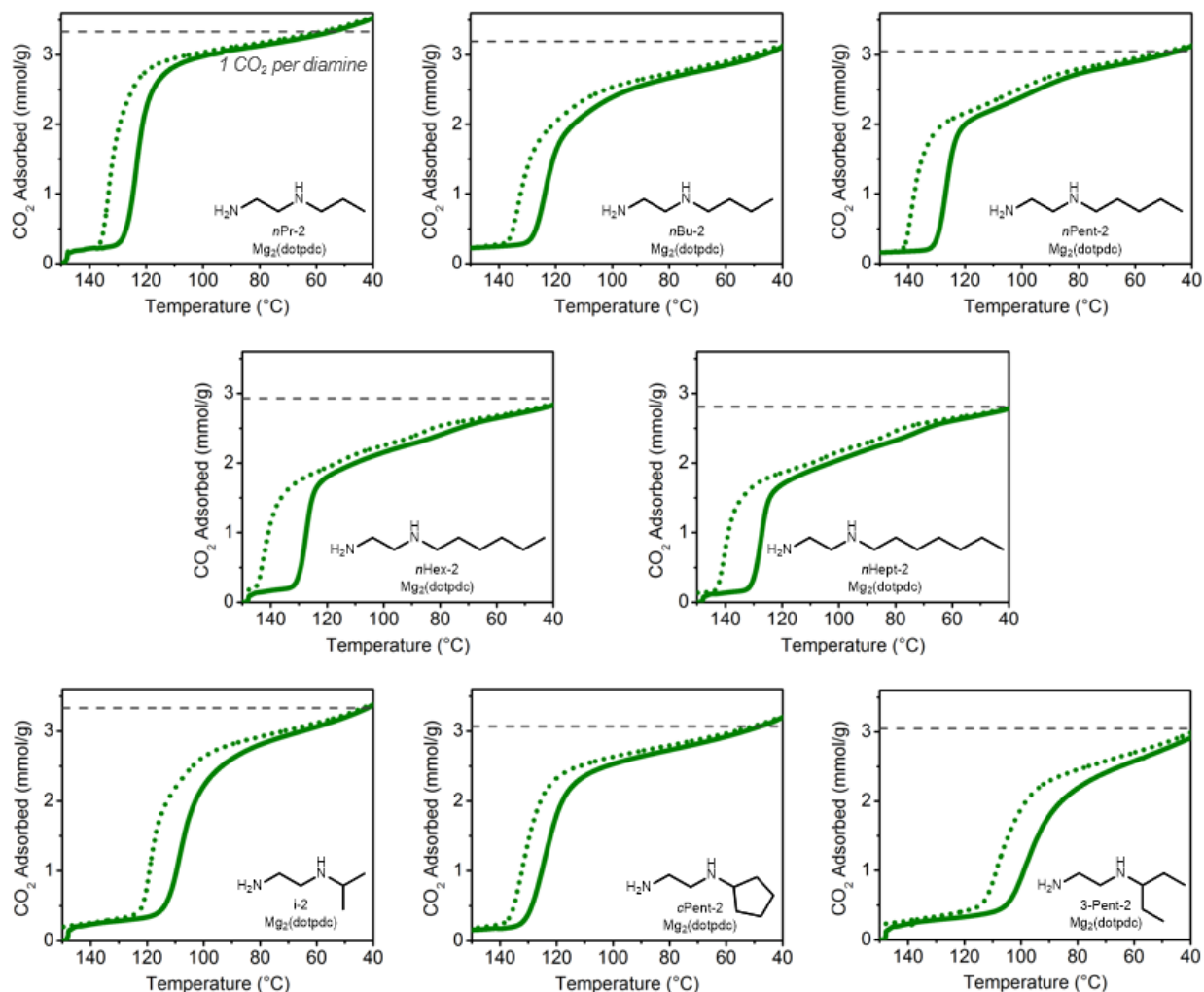
**Figure S25.** IR spectra of as-synthesized samples of 1°,2°-alkylethylenediamine-appended variants of  $\text{Mg}_2(\text{dotpdc})$ .



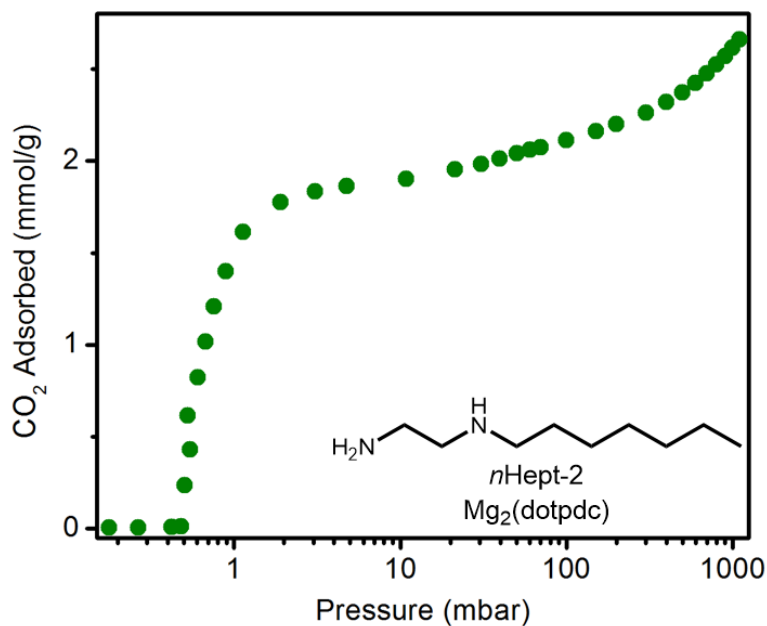
**Figure S26.** Dry N<sub>2</sub> decomposition profiles of 1°,2°-alkylethylenediamine-appended variants of Mg<sub>2</sub>(dotpdc). The rate of mass change at each temperature is shown in blue. A ramp rate of 1.5 °C/min was used.



**Figure S27.** Temperature of the maximum rate of diamine loss (determined from the plots in Figure S26) vs. diamine molecular weight for 1°,2°-alkylethylenediamine-appended variants of  $\text{Mg}_2(\text{dotpdc})$ , confirming that increasing the molecular weight of the diamine makes the adsorbent less susceptible to diamine loss.

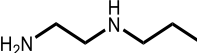
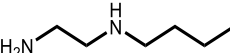
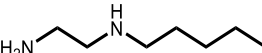
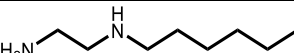
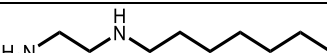
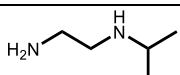
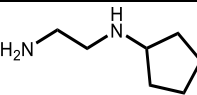
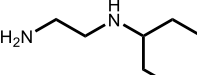


**Figure S28.** CO<sub>2</sub> adsorption (solid) and desorption (dotted) isobars under pure CO<sub>2</sub> for 1°,2°-alkylethylenediamine-appended variants of Mg<sub>2</sub>(dotpdc), confirming the lack of two CO<sub>2</sub> adsorption steps in all cases. A ramp rate of 2 °C/min was used.



**Figure S29.** 40 °C CO<sub>2</sub> isotherm of *n*Hept-2-Mg<sub>2</sub>(dotpdc), confirming the presence of only one CO<sub>2</sub> adsorption step at approximately 0.5 mbar.

**Table S4.** Typical diamine loadings and activation temperatures of 1°,2°-alkylethylenediamine-appended variants of Mg<sub>2</sub>(dotpdc).

Diamine	Diamine loading as synthesized	Activation temp. (°C)	Diamine loading after dry N <sub>2</sub> activation	Diamine loading after humid N <sub>2</sub> activation
	247%	150	96%	95%
	138%	170	90%	90%
	123%	180	95%	94%
	97%	150	89%	92%
	97%	150	n/d	93%
	156%	150	88%	89%
	134%	170	102%	100%
	105%	150	97%	91%

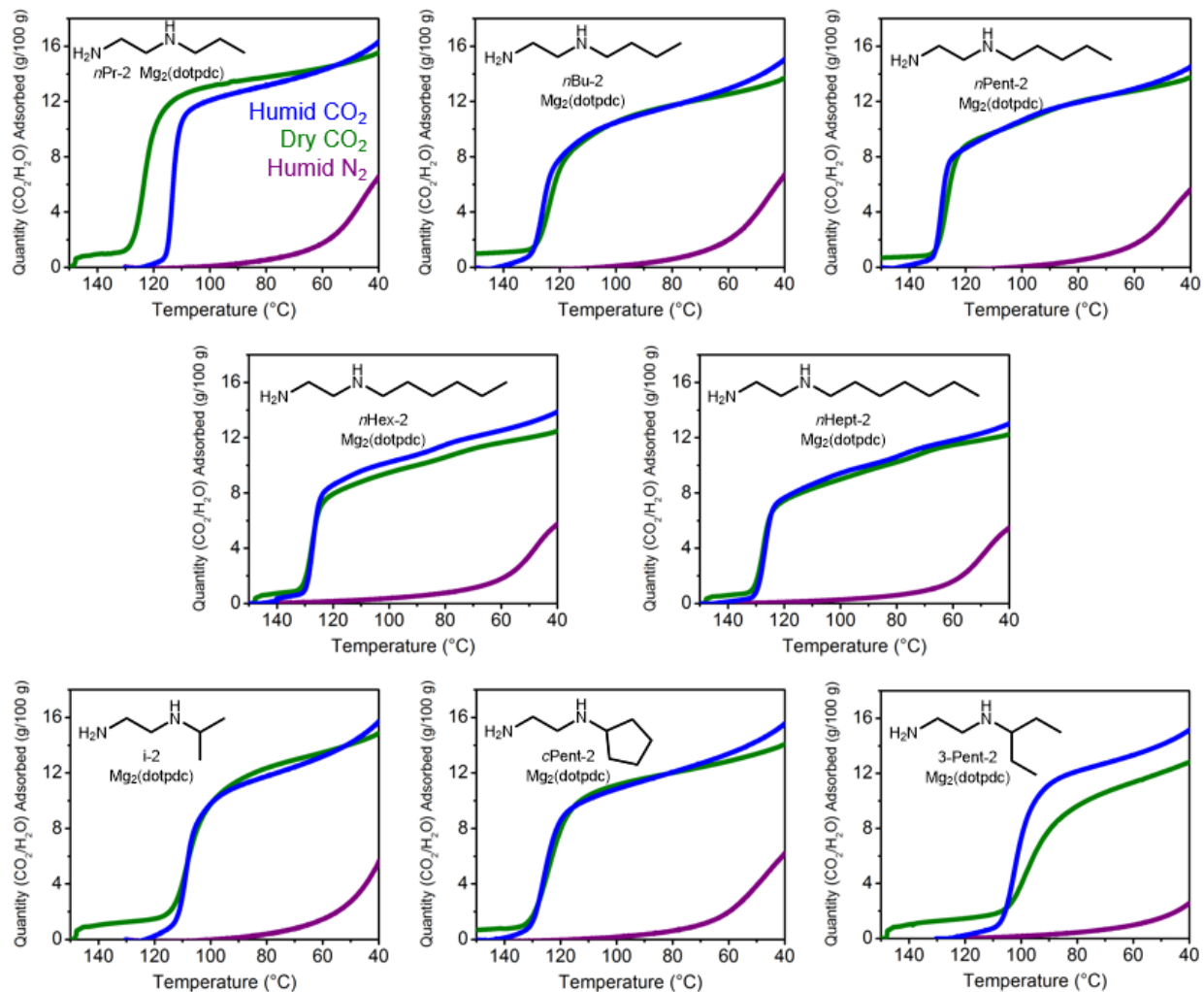


**Figure S30.** Humid  $\text{N}_2$  (purple), dry  $\text{CO}_2$  (green), and humid  $\text{CO}_2$  (blue) adsorption isobars of 1°,2°-alkylethylenediamine-appended variants of  $\text{Mg}_2(\text{dotpdc})$ . A ramp rate of 2 °C/min was used.

**Table S5.** Dry CO<sub>2</sub>, humid N<sub>2</sub>, and humid CO<sub>2</sub> capacities and estimated amounts of water co-adsorption for 1°,2°-alkylethylenediamine-appended variants of Mg<sub>2</sub>(dotpdc) at 40 °C, determined from isobaric cooling measurements (see Figure 9 in the main text).

Diamine	Dry CO <sub>2</sub> uptake (g/100 g)	Humid N <sub>2</sub> uptake (g/100 g)	Humid CO <sub>2</sub> uptake (g/100 g)	Estimated water co-adsorption (g/ 100 g)	Estimated water co-adsorption (per diamine)
	15.6	6.7	16.6	1.0	0.2
	13.8	6.9	15.3	1.5	0.3
	13.8	5.8	14.6	0.8	0.2
	12.5	5.8	14	1.5	0.3
	12.3	5.6	13.1	0.8	0.2
	14.9	6.4	16	1.1	0.2
	14.1	6.2	15.6	1.5	0.3
	14	2.6	15.1	1.1	0.2

## 7. *Primary,tertiary* (1°,3°) diamines appended to Mg<sub>2</sub>(dotpdc).

The preparation of ee-2-Mg<sub>2</sub>(dotpdc) was carried out using a slightly different procedure, which yielded material of higher crystallinity and CO<sub>2</sub> adsorption capacity than that prepared using the standard method outlined in the Experimental section. A 30 mL scintillation vial was charged with freshly-filtered methanol-solvated Mg<sub>2</sub>(dotpdc) (~20 mg) under N<sub>2</sub>. The vial was heated at 180 °C for 24 h under flowing N<sub>2</sub>. Meanwhile, freshly-ground CaH<sub>2</sub> (~30 mg) was added to a solution of 1 mL of *N,N*-diethylethylenediamine and 4 mL of toluene in a 30 mL scintillation vial equipped with a stir bar. The mixture was stirred at 100 °C under flowing N<sub>2</sub> for 30 min, at which time it was allowed to cool to room temperature and settle overnight. The dried diamine solution and activated Mg<sub>2</sub>(dotpdc) were transferred to a N<sub>2</sub>-filled glovebag, and the diamine solution was carefully added *via* syringe to the Mg<sub>2</sub>(dotpdc) sample, taking care not to disturb the CaH<sub>2</sub>. The vial was allowed to stand at room temperature for 24 h. At this time, the mixture was filtered, and the resulting powder was thoroughly washed with toluene (3 × 20 mL) and hexanes (3 × 20 mL) and allowed to dry on the filter paper for several minutes. Attempts to prepare high quality samples of pyrr-2-Mg<sub>2</sub>(dotpdc) have thus far been unsuccessful, yielding samples possessing poor crystallinity and broad CO<sub>2</sub> adsorption profiles.

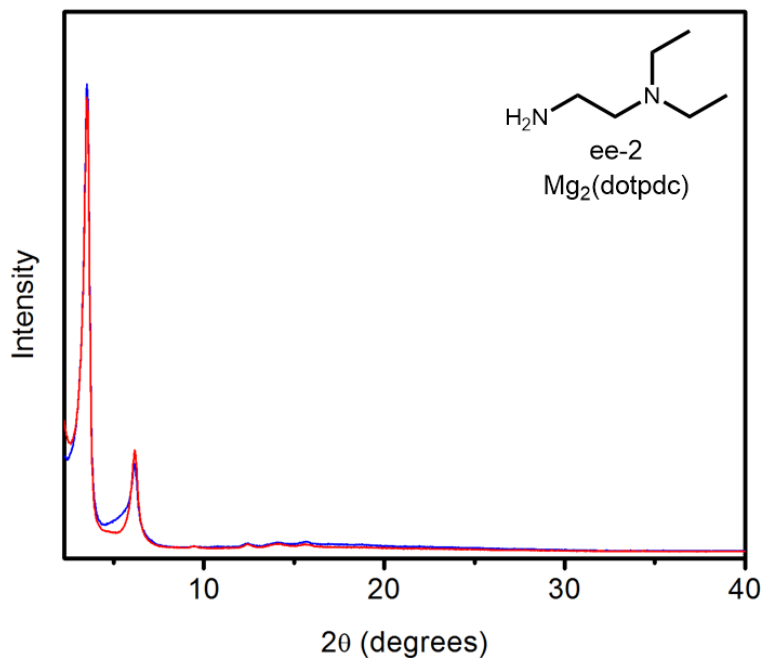


**Figure S31.** Powder X-ray diffraction patterns (CuK $\alpha$  radiation,  $\lambda = 1.5418 \text{ \AA}$ ) of as-synthesized (blue) and activated (red) ee-2–Mg<sub>2</sub>(dotpdc). The diamine loadings were found to be 133% upon synthesis and 98% after activation, as determined by <sup>1</sup>H NMR after digestion with DCl.

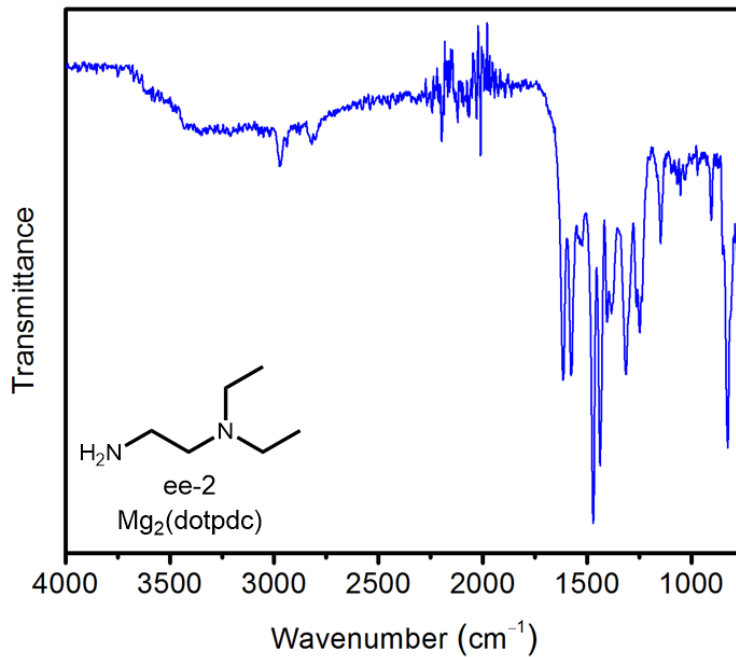


**Figure S32.** IR spectra of as-synthesized ee-2–Mg<sub>2</sub>(dotpdc).

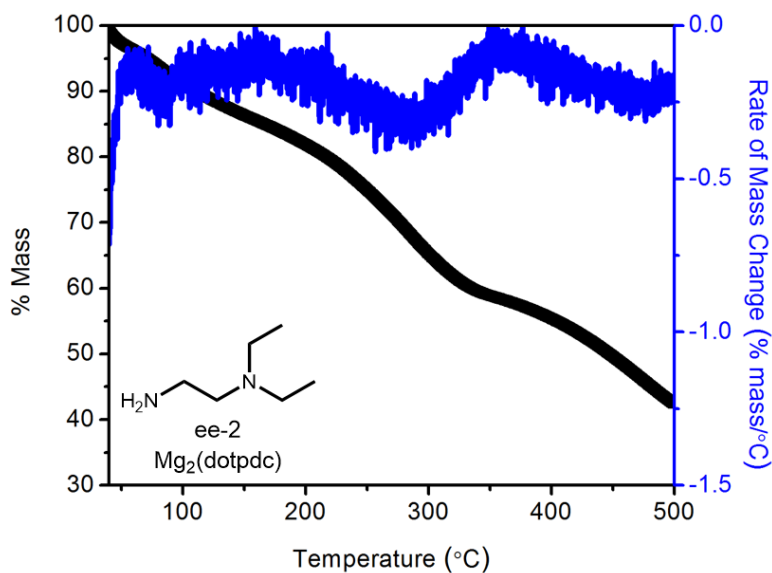


**Figure S33.** Dry N<sub>2</sub> decomposition profile of ee-2–Mg<sub>2</sub>(dotpdc). The rate of mass change at each temperature is shown in blue. A ramp rate of 1.5 °C/min was used.

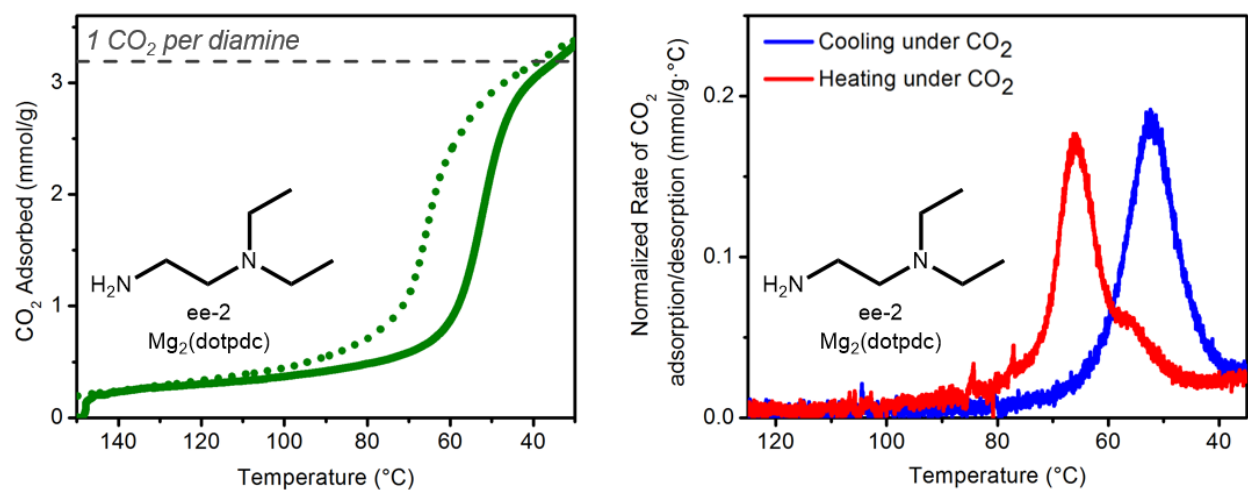


**Figure S34.** Left: CO<sub>2</sub> adsorption (solid line) and desorption (dotted line) isobars for ee-2–Mg<sub>2</sub>(dotpdc) appended. Right: The temperature derivative plots of these isobars show one CO<sub>2</sub> adsorption (blue) and desorption (red) step. A ramp rate of 2 °C/min was used.

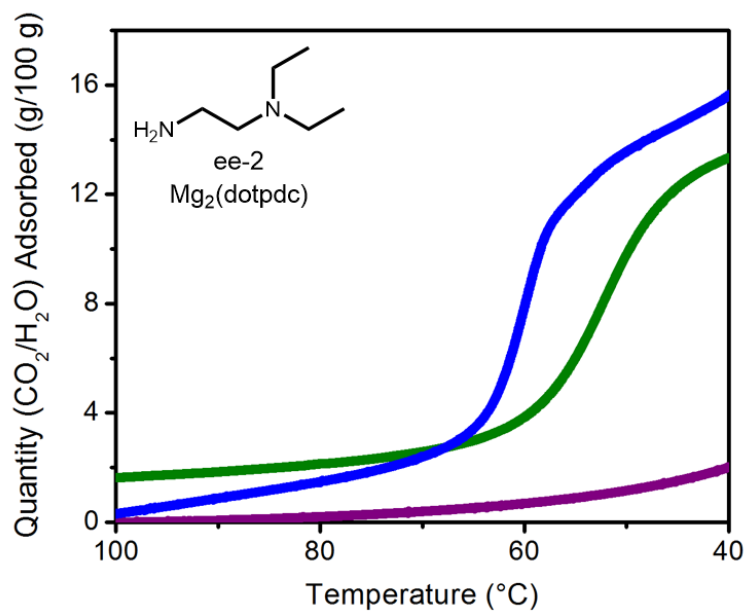
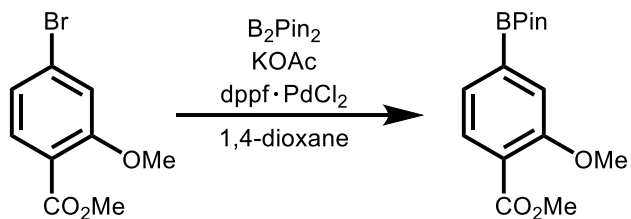


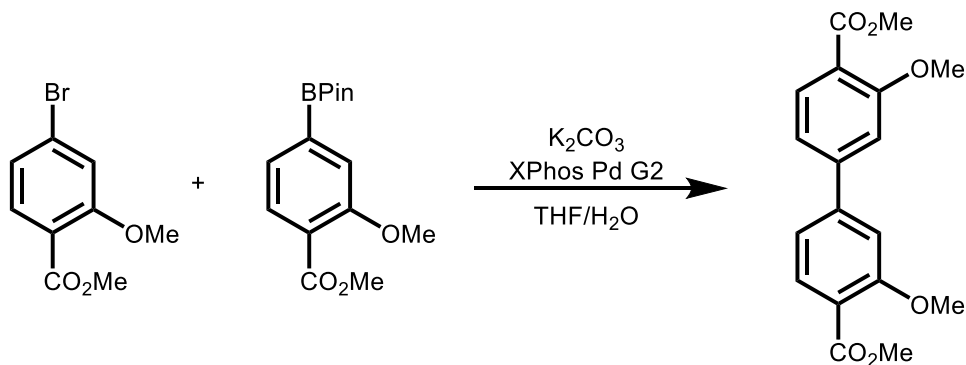
**Figure S35.** Humid N<sub>2</sub> (purple), dry CO<sub>2</sub> (green), and humid CO<sub>2</sub> (blue) adsorption isobars of ee-2-Mg<sub>2</sub>(dotpdc). The diamine loading was found to be 94% after the humid experiments, as determined by <sup>1</sup>H NMR after digestion with DCl. A ramp rate of 2 °C/min was used.

## 8. Preparation and characterization of Mg<sub>2</sub>(pc-dobpdc).

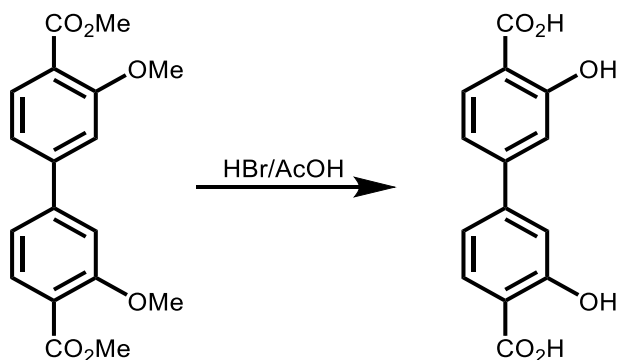
### Initial synthesis of H<sub>4</sub>pc-dobpdc:



A 500 mL 3-neck roundbottom flask equipped with a stir bar and reflux condenser was charged with methyl 4-bromo-2-methoxybenzoate (10.0 g, 40.8 mmol, 1.00 eq.), bis(pinacolato)diboron (13.5 g, 53.1 mmol, 1.30 eq.), potassium acetate (12.0 g, 122 mmol, 3.00 eq.), and bis(diphenylphosphino)ferrocene]dichloropalladium(II) complex with dichloromethane (1.67 g, 2.04 mmol, 0.05 eq.). The flask was evacuated under high vacuum and back-filled with Ar. This process was repeated a total of three times. Next, degassed 1,4-dioxane (200 mL) was added, and the reaction mixture was allowed to stir at reflux for 16 h. At this time, the reaction mixture was cooled to room temperature and filtered. The filtrate was concentrated *in vacuo* and a stir bar, ethyl acetate (500 mL), and activated charcoal (~10 g) were added to the resulting residue. The flask was equipped with a reflux condenser, and the mixture was allowed to stir at reflux for 1 h. The reaction mixture was cooled to room temperature and filtered through a celite plug, eluting with ethyl acetate (500 mL). The filtrate was concentrated *in vacuo* to yield a brown oil. This oil was dissolved in 1:2 ethyl acetate in hexanes (30 mL) and flushed through a short silica gel plug, eluting with 1:2 ethyl acetate in hexanes (250 mL). The filtrate was concentrated *in vacuo*. The resulting solid was recrystallized from hexanes to yield methyl 2-methoxy-4-(4,4,5,5-tetramethyl-1,3,2-dioxaborolan-2-yl)benzoate (9.90 g, 83% over four crops) as an off-white solid. <sup>1</sup>H NMR (400 MHz, CDCl<sub>3</sub>): δ 7.75 (d, J = 8 Hz, 1H), 7.40 (d, J = 8 Hz, 1H), 7.37 (s, 1H), 3.94 (s, 3H), 3.88 (s, 3H), 1.35 (s, 12H) ppm.



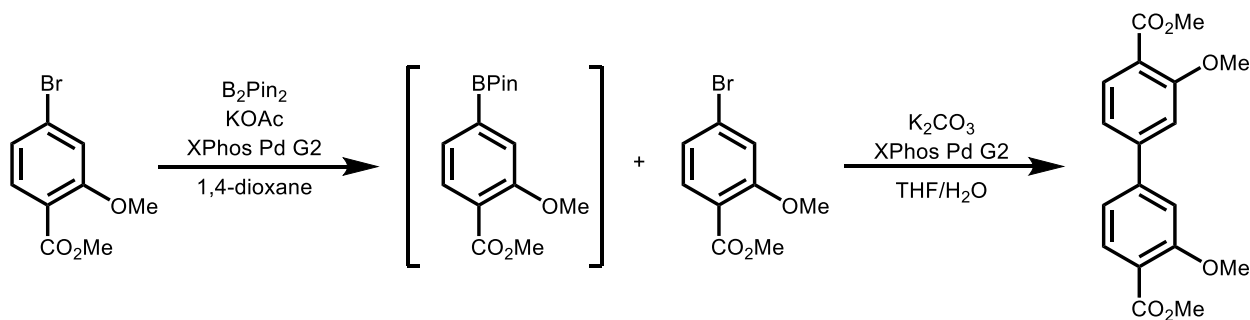
A 500 mL roundbottom flask equipped with a reflux condenser and stir bar was charged with methyl 4-bromo-2-methoxybenzoate (3.19 g, 13.0 mmol, 1.00 eq.), methyl 2-methoxy-4-(4,4,5,5-tetramethyl-1,3,2-dioxaborolan-2-yl)benzoate (4.20 g, 14.4 mmol, 1.10 eq.), potassium carbonate (17.3 g, 125 mmol, 9.60 eq.), and XPhos Pd G2<sup>5</sup> (257 mg, 0.33 mmol, 2.50%). The flask was sparged with Ar for 1 h, at which time a degassed 4:1 solution of THF and water (350 mL) was added. The reaction mixture was allowed to stir at reflux for 48 h. The THF was removed *in vacuo*, and the non-homogenous solution was filtered. The resulting black solid was suspended in ethyl acetate (750 mL) and filtered, which yielded dimethyl 3,3'-dimethoxy-[1,1'-biphenyl]-4,4'-dicarboxylate (2.50 g, 58%) as an off-white solid. The filtrate was concentrated, and the resulting residue was recrystallized from ethyl acetate (50 mL) and chloroform (10 mL) to yield additional dimethyl 3,3'-dimethoxy-[1,1'-biphenyl]-4,4'-dicarboxylate (1.38 g, 32%) as an off-white solid (combined yield: 90%). <sup>1</sup>H NMR (300 MHz,  $CDCl_3$ ):  $\delta$  7.90 (d,  $J$  = 8 Hz, 1H), 7.20 (dd,  $J$  = 8, 2 Hz, 1H), 7.15 (d,  $J$  = 2 Hz, 1H), 3.99 (s, 3H), 3.92 (s, 3H) ppm.



A 500 mL roundbottom flask equipped with a reflux condenser and stir bar was charged with dimethyl 3,3'-dimethoxy-[1,1'-biphenyl]-4,4'-dicarboxylate (2.40g, 7.27 mmol, 1.00 eq.), glacial acetic acid (90 mL), and concentrated hydrobromic acid (90 mL). The mixture was allowed to stir at reflux for 48 h, at which time it was cooled to room temperature and poured into ice water (400 mL). The mixture was filtered, and the resulting white solid was washed thoroughly with water (3 L) to yield 3,3'-dihydroxy-[1,1'-biphenyl]-4,4'-dicarboxylic acid (1.80 g, 90%) as a white solid.  $^1\text{H}$  NMR (300 MHz, DMSO- $d_6$ ):  $\delta$  11.4 (bs, 2H), 7.88 (d,  $J$  = 9 Hz, 1H), 7.25-7.32 (m, 2H) ppm;  $^{13}\text{C}$  NMR (100 MHz, DMSO- $d_6$ ):  $\delta$  171.7, 161.4, 145.6, 130.9, 118.0, 115.3, 112.8 ppm. These spectra are consistent with those previously reported in the literature.<sup>6</sup>

#### Large-scale synthesis of H<sub>4</sub>pc-dobpdc:

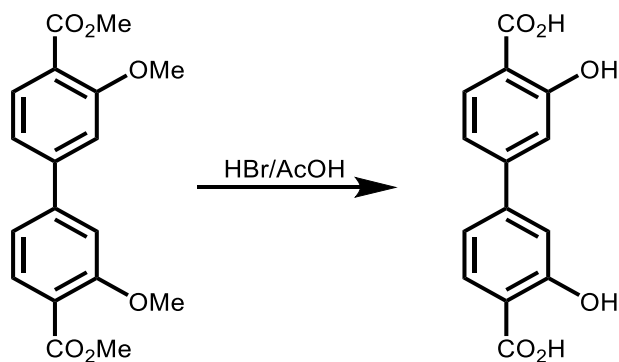
Several slight modifications to the above procedure allowed for the convenient preparation of H<sub>4</sub>pc-dobpdc on a nearly 10 g scale.



A 500 mL 3-neck roundbottom flask equipped with a stir bar and reflux condenser was charged with methyl 4-bromo-2-methoxybenzoate (10.0 g, 40.8 mmol, 1.00 eq.), bis(pinacolato)diboron (13.5 g, 53.1 mmol, 1.30 eq.), potassium acetate (12.0 g, 122 mmol, 3.00 eq.), and XPhos Pd G2<sup>5</sup> (642 mg, 0.82 mmol, 0.02 eq.). The flask was evacuated under high vacuum and back-filled with N<sub>2</sub>. This process was repeated a total of three times. Next, degassed 1,4-dioxane (100 mL) was added, and the reaction mixture was allowed to stir at reflux for 16 h.

At this time, the reaction mixture was cooled to room temperature and the solvent was removed *in vacuo*. The resulting brown oil was dissolved in CH<sub>2</sub>Cl<sub>2</sub> (100 mL) and filtered through celite, eluting with CH<sub>2</sub>Cl<sub>2</sub> (400 mL). The filtrate was concentrated *in vacuo* to produce a brown oil. Hexanes (50 mL) was added and removed *in vacuo*; this process was repeated a total of three times to remove residual CH<sub>2</sub>Cl<sub>2</sub>. At this stage, <sup>1</sup>H NMR analysis of the crude product (13.6 g) confirmed it consisted primarily of the desired methyl 2-methoxy-4-(4,4,5,5-tetramethyl-1,3,2-dioxaborolan-2-yl)benzoate and residual pinacol, and thus it was used directly in the next step without further purification.

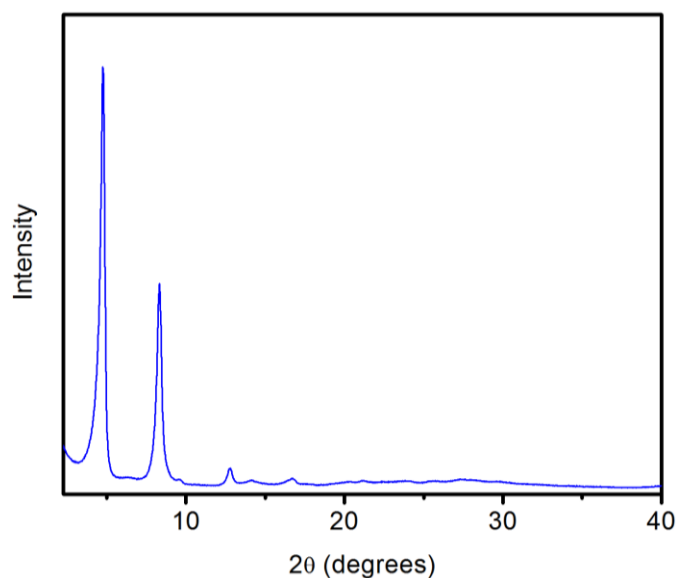
A 250 mL 3-neck roundbottom flask equipped with a reflux condenser and stir bar was charged with methyl 4-bromo-2-methoxybenzoate (9.72 g, 39.6 mmol, 1.00 eq.) and XPhos Pd G2<sup>5</sup> (623 mg, 0.79 mmol, 0.02 eq.). The flask was evacuated under high vacuum and back-filled with N<sub>2</sub>. This process was repeated a total of three times. Meanwhile, crude 2-methoxy-4-(4,4,5,5-tetramethyl-1,3,2-dioxaborolan-2-yl)benzoate (13.6 g, ~1 eq.) was dissolved in THF (40 mL), and potassium carbonate (11.0 g, 79.2 mmol, 2.00 eq.) was dissolved in deionized water (80 mL). The two solutions were sparged with N<sub>2</sub> for 1 h. At this time, the THF solution was added to the 3-neck flask, followed by the aqueous solution. The reaction mixture was allowed to stir at reflux for 14 h, which resulted in precipitation of a gray solid from solution. Water (100 mL) was added, and the reaction mixture was filtered. The resulting gray solid was dissolved in hot CH<sub>2</sub>Cl<sub>2</sub> (200 mL) and filtered through celite, eluting with CH<sub>2</sub>Cl<sub>2</sub> (500 mL). The solvent was removed *in vacuo*. The resulting dark gray solid was triturated from cold methanol and filtered, yielding dimethyl 3,3'-dimethoxy-[1,1'-biphenyl]-4,4'-dicarboxylate (10.6 g, 81%) as a pale gray solid. This product was identical to that prepared on smaller scale by <sup>1</sup>H NMR (300 MHz, CDCl<sub>3</sub>) analysis.



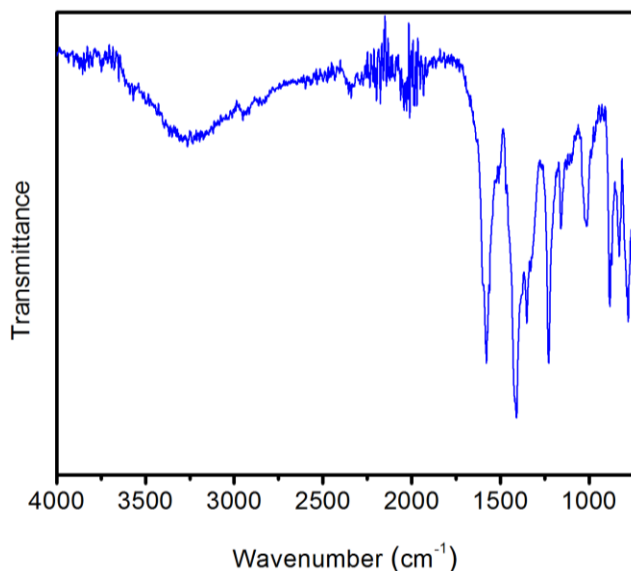
A 1 L roundbottom flask equipped with a reflux condenser and stir bar was charged with dimethyl 3,3'-dimethoxy-[1,1'-biphenyl]-4,4'-dicarboxylate (10.6 g, 32.1 mmol, 1.00 eq.), glacial acetic acid (300 mL), and concentrated hydrobromic acid (300 mL). The mixture was allowed to stir at reflux for 48 h, during which time a white solid precipitated from the dark brown solution. The mixture was filtered, and the resulting white solid was washed thoroughly with water (2 L) to yield 3,3'-dihydroxy-[1,1'-biphenyl]-4,4'-dicarboxylic acid (8.37 g, 95%) as an off-white solid. This product was identical to that prepared on smaller scale by <sup>1</sup>H NMR (300 MHz, DMSO-d<sub>6</sub>) analysis.

**Synthesis of Mg-IRMOF-74-II or Mg<sub>2</sub>(pc-dobpdc):** A 20 mL scintillation vial was charged with 3,3'-dihydroxy-[1,1'-biphenyl]-4,4'-dicarboxylic acid (26.0 mg, 95.0 μmol, 1.00 equiv.) and Mg(NO<sub>3</sub>)<sub>2</sub>·6H<sub>2</sub>O (80.0 mg, 0.310 mmol, 3.10 equiv.). Fresh *N,N*-dimethylformamide (DMF) (7.5 mL) was added, and the solution was sonicated until all of the solids dissolved. Next, 0.5 mL of ethanol and 0.5 mL of deionized water were added. The vial was wrapped in Teflon tape, sealed, and heated at 120 °C in a heating block for 24 h, during which time an off-white solid precipitated from solution. The solution was filtered while still hot, and the resulting solid was washed with fresh DMF (15 mL). The filtrate was transferred to a vial and soaked in fresh DMF (10 mL) at 60 °C for 3 h. The supernatant was decanted and replaced with fresh DMF (10 mL), and the vial was re-heated to 60 °C. This washing process was repeated a total of three times. The DMF was

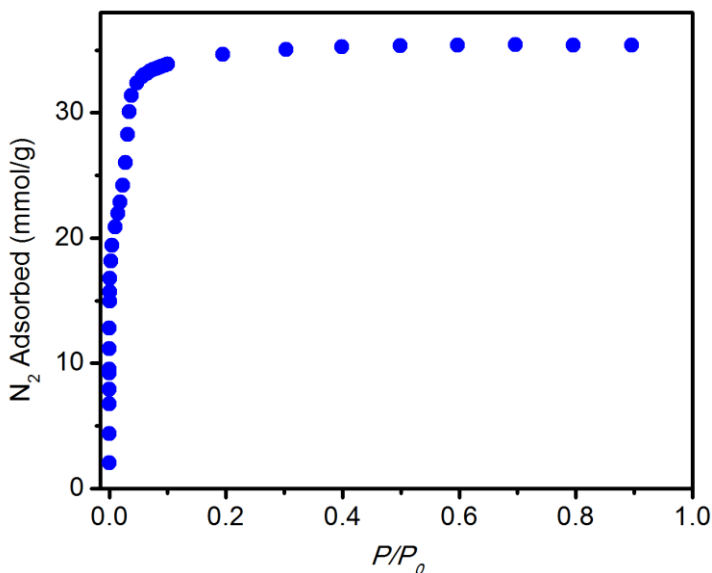
replaced with methanol (10 mL), and the off-white solid was soaked in methanol at 60 °C for 3 h. The supernatant was decanted and replaced with fresh methanol (10 mL), and the vial was reheated to 60 °C. This washing process was repeated a total of three times. Activation of the resulting powder at 180 °C under flowing N<sub>2</sub> for 14 h and then under reduced pressure (<10 μbar) at 180 °C for 24 h afforded Mg<sub>2</sub>(pc-dobpdc) as a pale yellow powder. The PXRD pattern, IR spectrum, and 77K N<sub>2</sub> adsorption isotherm for this material are consistent with those previously reported.<sup>6</sup> Large scale batches of Mg<sub>2</sub>(pc-dobpdc) were prepared by combining the product from multiple 20 mL scintillation vials prior to washing.



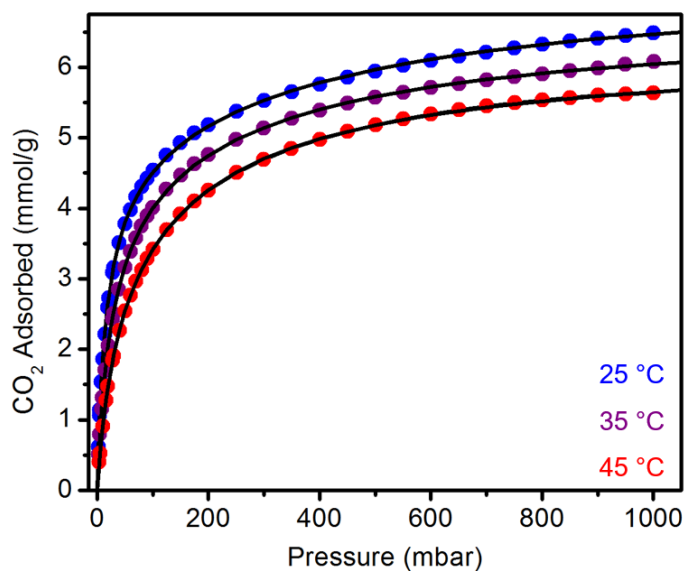
**Figure S36.** Powder X-ray diffraction pattern (CuK $\alpha$  radiation,  $\lambda = 1.5418 \text{ \AA}$ ) of MeOH-solvated Mg<sub>2</sub>(pc-dobpdc). This pattern is consistent with that previously reported for the activated framework.<sup>6</sup>



**Figure S37.** IR spectrum of MeOH-solvated  $\text{Mg}_2(\text{pc-dobpdc})$ , confirming that washing with MeOH is sufficient to remove  $N,N$ -dimethylformamide from the open  $\text{Mg}^{2+}$  sites.



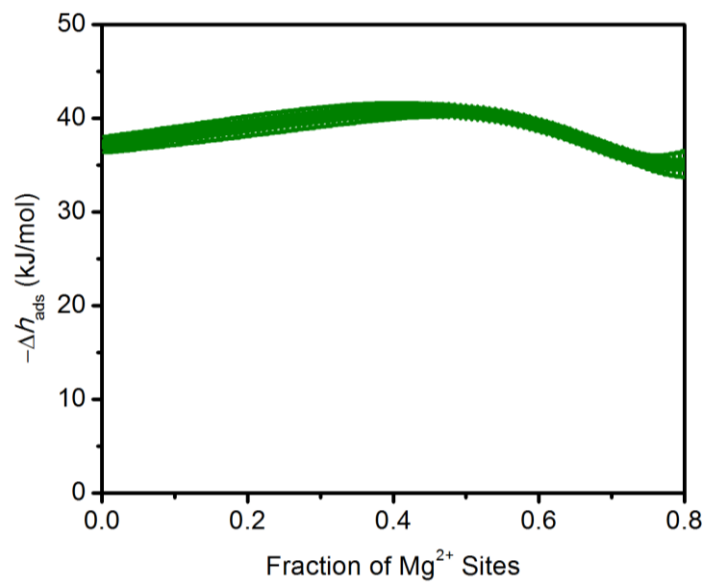
**Figure S38.** 77K  $\text{N}_2$  adsorption isotherm of activated  $\text{Mg}_2(\text{pc-dobpdc})$ . Fitting these data yielded a Brunauer–Emmett–Teller surface area of  $3000 \pm 90 \text{ m}^2/\text{g}$ , significantly higher than that previously reported ( $2510 \text{ m}^2/\text{g}$ ) for this framework.<sup>6</sup> The higher surface area compared to that previously reported is attributed to the different washing procedure employed herein. The surface area of  $\text{Mg}_2(\text{pc-dobpdc})$  is slightly lower than that of  $\text{Mg}_2(\text{dobpdc})$  ( $3330 \text{ m}^2/\text{g}$ ),<sup>7</sup> likely due to the smaller pore diameter of  $\text{Mg}_2(\text{pc-dobpdc})$  ( $17 \text{ \AA}$ )<sup>6</sup> compared to that of  $\text{Mg}_2(\text{dobpdc})$  ( $19 \text{ \AA}$ )<sup>4</sup> and not due to incomplete activation. The Langmuir surface area of  $\text{Mg}_2(\text{pc-dobpdc})$  determined from this isotherm is  $3470 \text{ m}^2/\text{g}$ .



**Figure S39.** 25 (blue), 35 (purple), and 45 °C (red) CO<sub>2</sub> isotherms of activated Mg<sub>2</sub>(pc-dobpdc). Independently fit dual-site Langmuir-Freundlich models are shown.

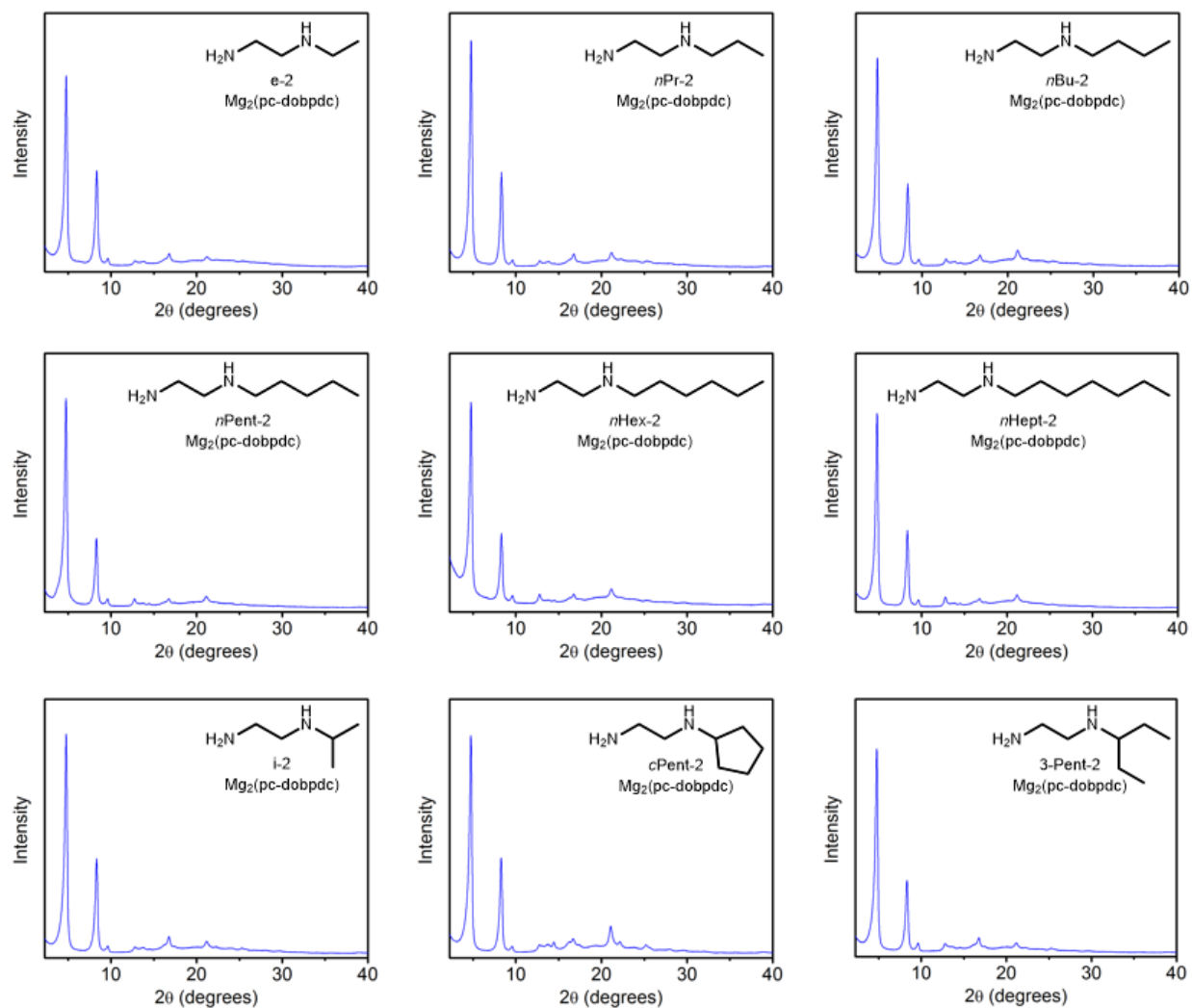
**Table S6.** Dual-site Langmuir-Freundlich parameters for the independently fit CO<sub>2</sub> isotherms of Mg<sub>2</sub>(pc-dobpdc) at 25, 35, and 45 °C.

Parameter	25 °C	35 °C	45 °C
$q_{sat1}$ (mmol/g)	4.61	4.07	3.14
$b_1$ (bar <sup>-1</sup> )	62.4	43.0	31.7
$v_1$	1	1	1
$q_{sat2}$ (mmol/g)	2.72	2.64	3.14
$b_2$ (bar <sup>-1</sup> )	2.45	3.58	4.83
$v_2$	1	1	1

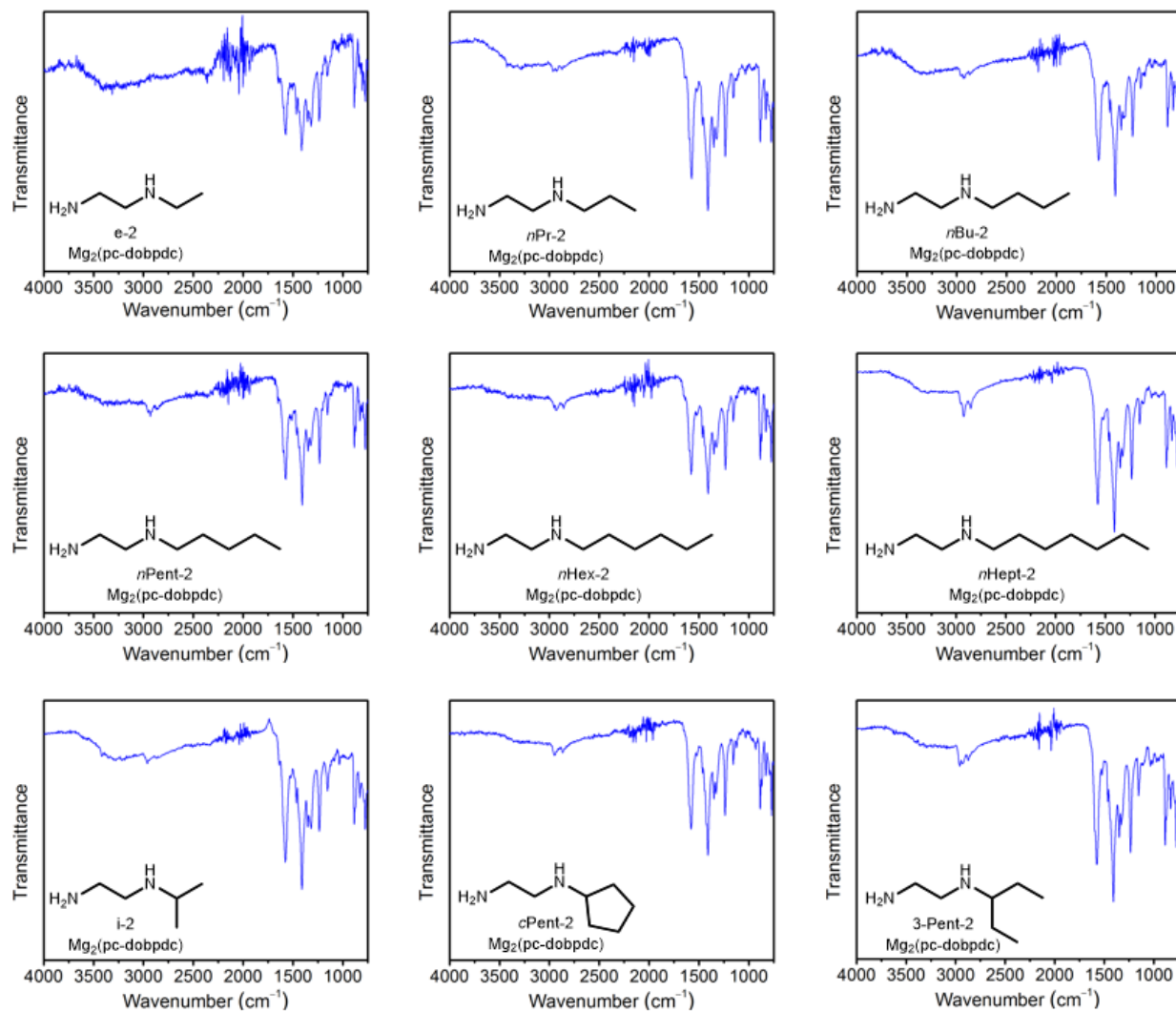


**Figure S40.**  $\text{CO}_2$  differential heats of adsorption as a function of fraction of occupied metal sites in activated  $\text{Mg}_2(\text{pc-dobpdc})$ . The differential heat of adsorption at low loadings ( $\sim 38$  kJ/mol) is similar to that previously reported for  $\text{Mg}_2(\text{dobpdc})$  ( $\sim 44$  kJ/mol)<sup>4</sup> and reported above for  $\text{Mg}_2(\text{dotpdc})$  ( $\sim 40$  kJ/mol).

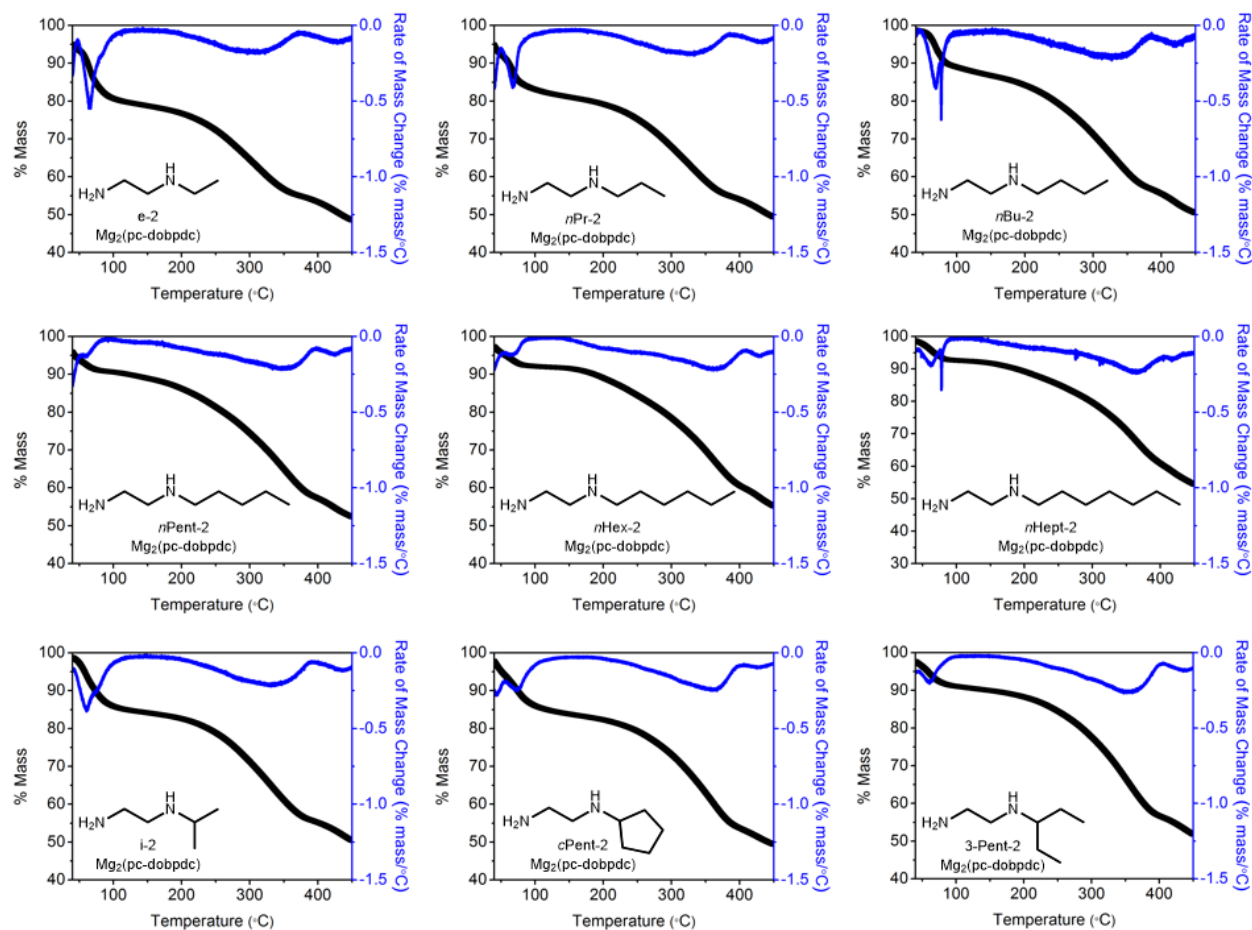
## 9. Primary,secondary (1°,2°) diamines appended to Mg<sub>2</sub>(pc-dobpdc).



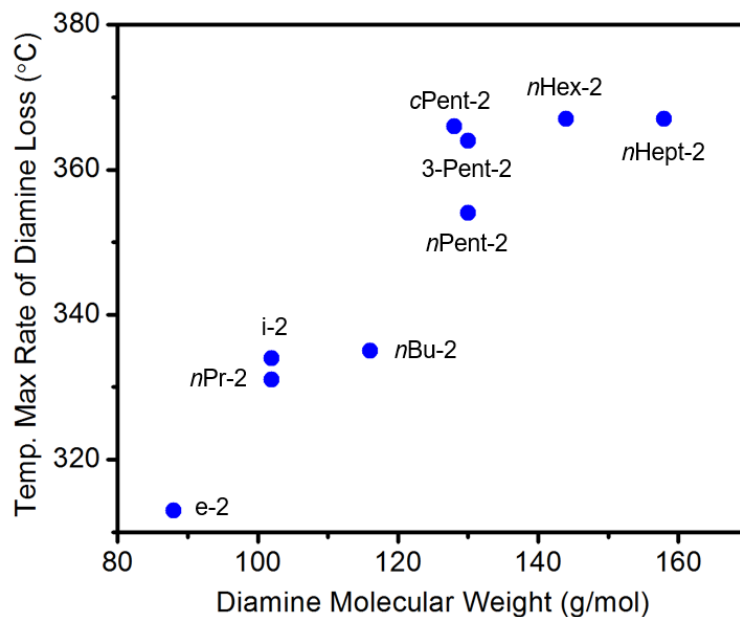
**Figure S41.** Powder X-ray diffraction patterns (CuK $\alpha$  radiation,  $\lambda = 1.5418 \text{ \AA}$ ) of as-synthesized samples of 1°,2°-alkylethylenediamine-appended variants of Mg<sub>2</sub>(pc-dobpdc).



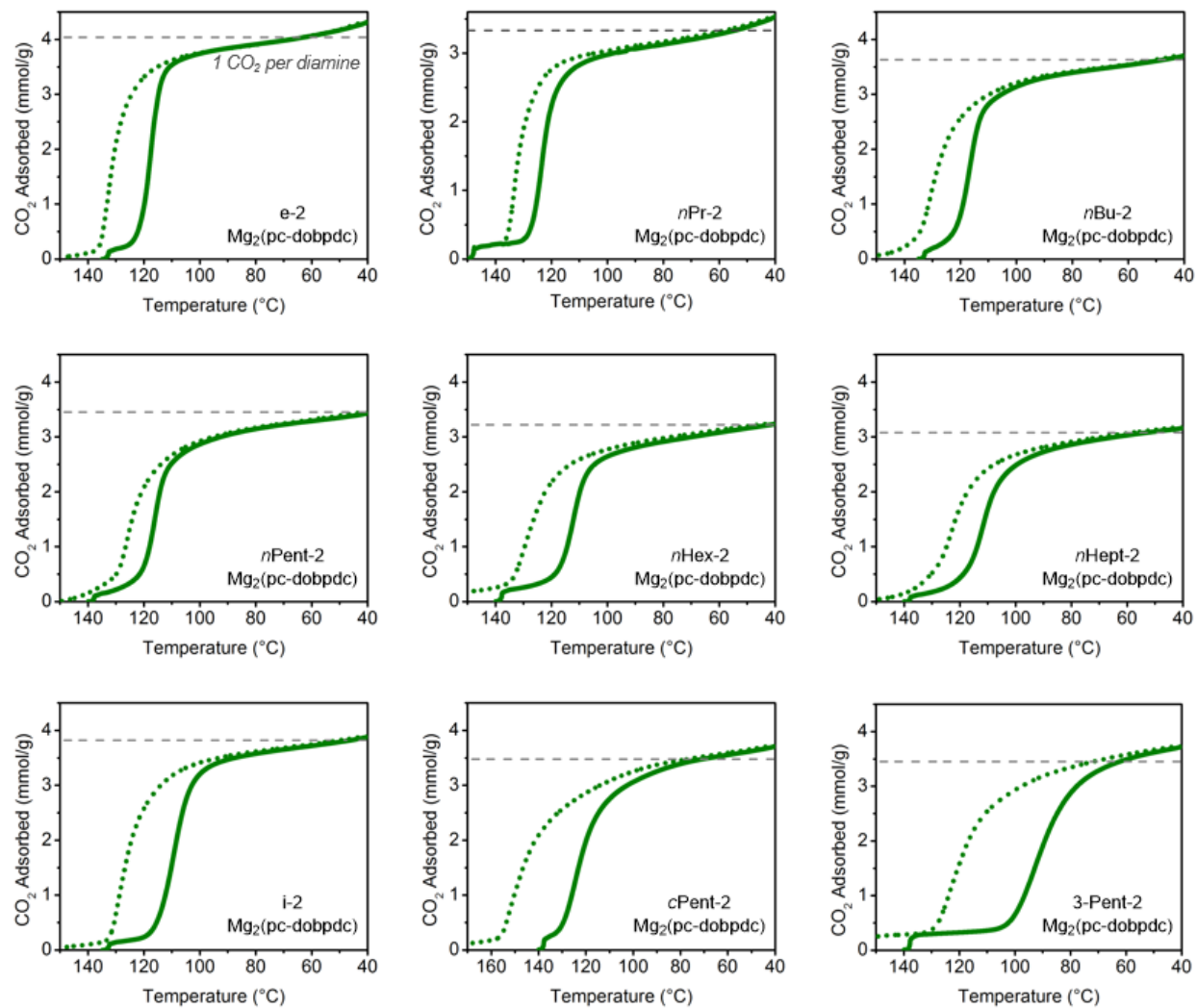
**Figure S42.** IR spectra of as-synthesized samples of 1°,2°-alkylethylenediamine-appended variants of Mg<sub>2</sub>(pc-dobpdc).



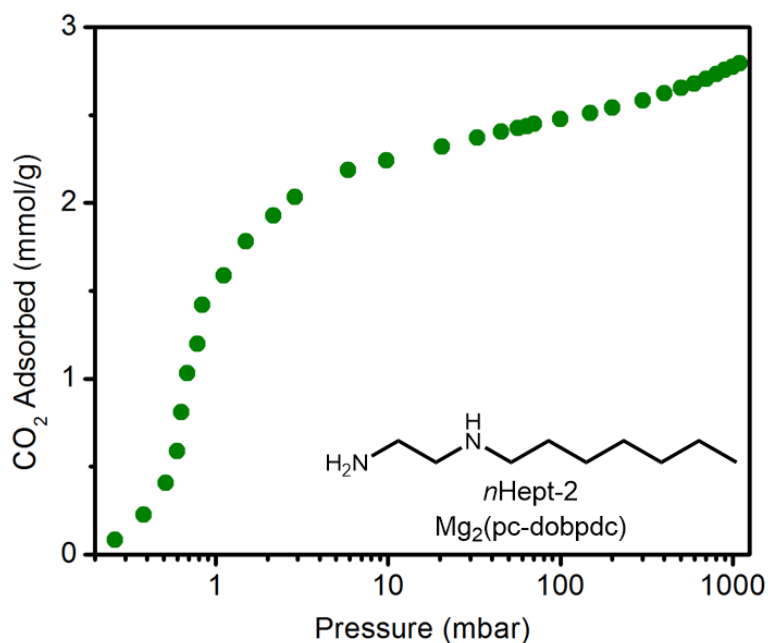
**Figure S43.** Dry N<sub>2</sub> decomposition profiles of 1°,2°-alkylethylenediamine-appended variants of Mg<sub>2</sub>(pc-dobpdc). The rate of mass change at each temperature is shown in blue. A ramp rate of 1.5 °C/min was used.



**Figure S44.** Temperature of the maximum rate of diamine loss (determined from the plots in Figure S43) vs. diamine molecular weight for 1°,2°-alkylethylenediamine-appended variants of  $\text{Mg}_2(\text{pc-dobpdc})$ , confirming that increasing the molecular weight of the diamine makes the adsorbent less susceptible to diamine loss.



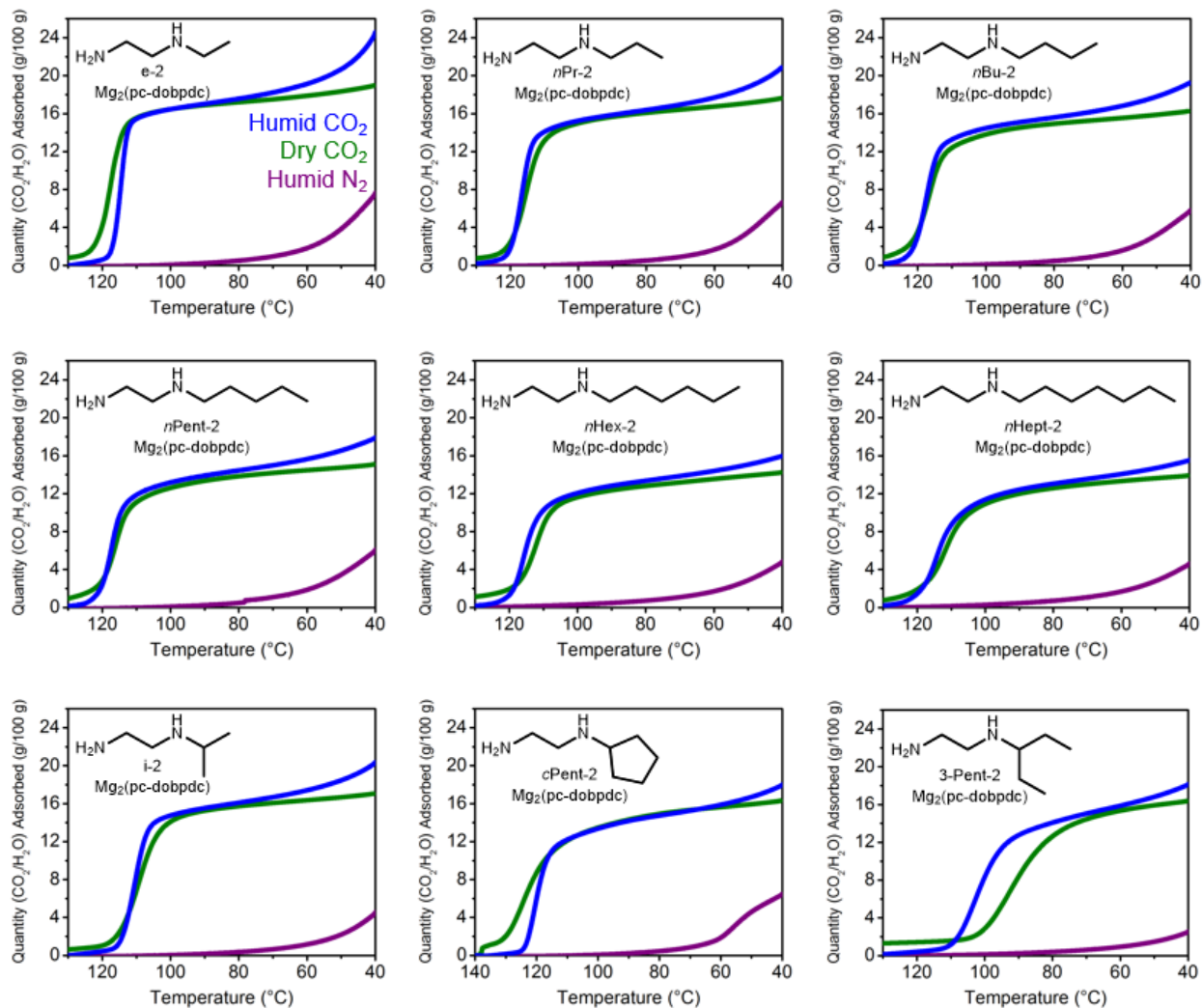
**Figure S45.** CO<sub>2</sub> adsorption (solid) and desorption (dotted) isobars under pure CO<sub>2</sub> for 1°,2°-alkylethylenediamine-appended variants of Mg<sub>2</sub>(pc-dobpdc), confirming the lack of two CO<sub>2</sub> adsorption steps in all cases. A ramp rate of 2 °C/min was used.



**Figure S46.** 40 °C CO<sub>2</sub> isotherm of *n*Hept-2-Mg<sub>2</sub>(pc-dobpdc), confirming the presence of only one CO<sub>2</sub> adsorption step at approximately 0.7 mbar.

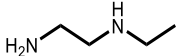
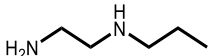
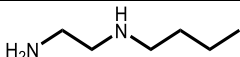
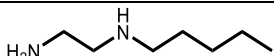
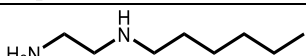
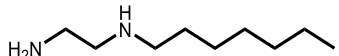
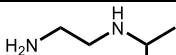
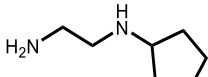
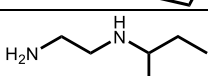
**Table S7.** Typical diamine loadings and activation temperatures of 1°,2°-alkylethylenediamine-appended variants of Mg<sub>2</sub>(pc-dobpdc).

Diamine	Diamine loading as synthesized	Activation temp. (°C)	Diamine loading after humid N <sub>2</sub> activation
	115%	120	97%
	105%	120	96%
	101%	135	98%
	104%	140	100%
	89%	140	91%
	79%	140	80%
	104%	120	95%
	100%	140	96%
	95%	140	92%



**Figure S47.** Humid  $\text{N}_2$  (purple), dry  $\text{CO}_2$  (green), and humid  $\text{CO}_2$  (blue) isobars of 1°,2°-alkylethylenediamine-appended variants of  $\text{Mg}_2(\text{pc-dobpdc})$ . A ramp rate of 2 °C/min was used.

**Table S8.** Dry CO<sub>2</sub>, humid N<sub>2</sub>, and humid CO<sub>2</sub> capacities and estimated amounts of water co-adsorption for 1°,2°-alkylethylenediamine-appended variants of Mg<sub>2</sub>(pc-dobpdc) at 40 °C, determined from isobaric cooling measurements (see Figure 13 in the main text).

Diamine	Dry CO <sub>2</sub> uptake (g/100 g)	Humid N <sub>2</sub> uptake (g/100 g)	Humid CO <sub>2</sub> uptake (g/100 g)	Estimated water co-adsorption (g/ 100 g)	Estimated water co-adsorption (per diamine)
	19.0	7.6	24.6	5.6	0.8
	17.6	6.6	20.9	3.3	0.5
	16.3	5.8	19.2	2.9	0.5
	15.1	5.8	17.9	2.8	0.5
	14.2	4.9	16.0	1.8	0.3
	13.9	4.6	15.6	1.7	0.3
	17.1	4.5	20.4	3.3	0.5
	16.3	6.5	18.0	1.7	0.3
	16.4	2.6	18.2	1.8	0.3

## 10. Primary, tertiary (1°, 3°) diamines appended to Mg<sub>2</sub>(pc-dobpdc).

The frameworks ee-2-Mg<sub>2</sub>(pc-dobpdc) and pyrr-2-Mg<sub>2</sub>(pc-dobpdc) were prepared according to the procedure outlined in the Experimental section.

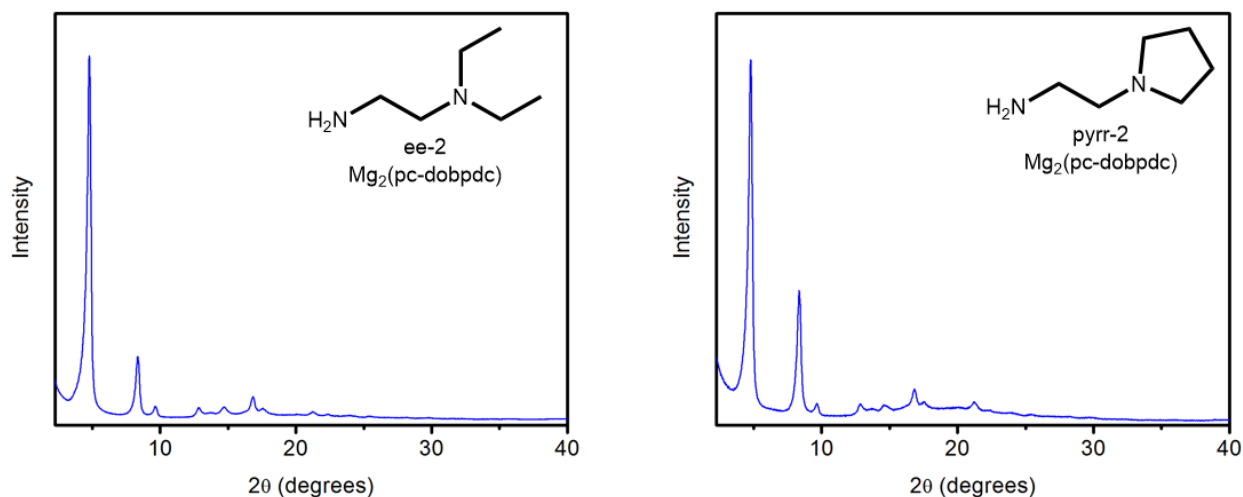


**Figure S48.** Powder X-ray diffraction patterns (CuKα radiation,  $\lambda = 1.5418 \text{ \AA}$ ) of as-synthesized samples of ee-2-Mg<sub>2</sub>(pc-dobpdc) (left) and pyrr-2-Mg<sub>2</sub>(pc-dobpdc) (right). The diamine loadings of these samples were found to be 102% and 108%, respectively, as determined by <sup>1</sup>H NMR after digestion with DCl.

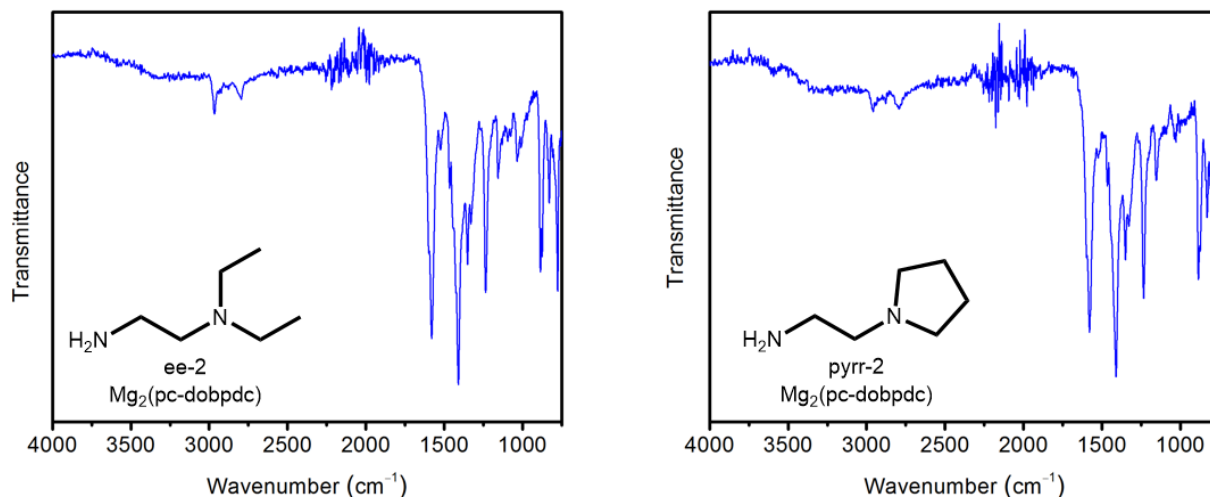


**Figure S49.** IR spectra of as-synthesized samples of ee-2-Mg<sub>2</sub>(pc-dobpdc) (left) and pyrr-2-Mg<sub>2</sub>(pc-dobpdc) (right).

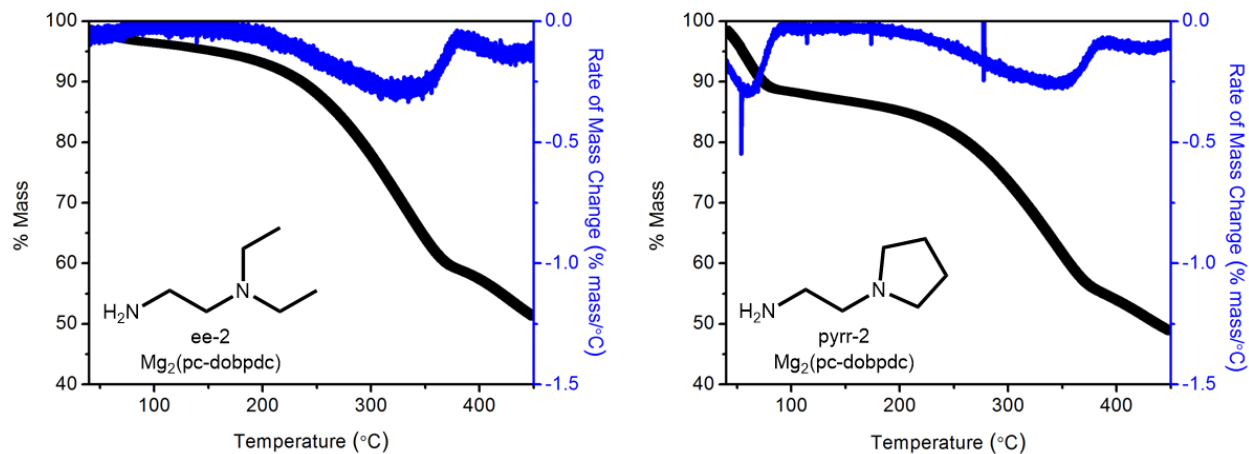


**Figure S50.** Dry N<sub>2</sub> decomposition profiles of ee-2-Mg<sub>2</sub>(pc-dobpdc) (left) and pyr-2-Mg<sub>2</sub>(pc-dobpdc) (right). The rate of mass change at each temperature is shown in blue. A ramp rate of 1.5 °C/min was used.

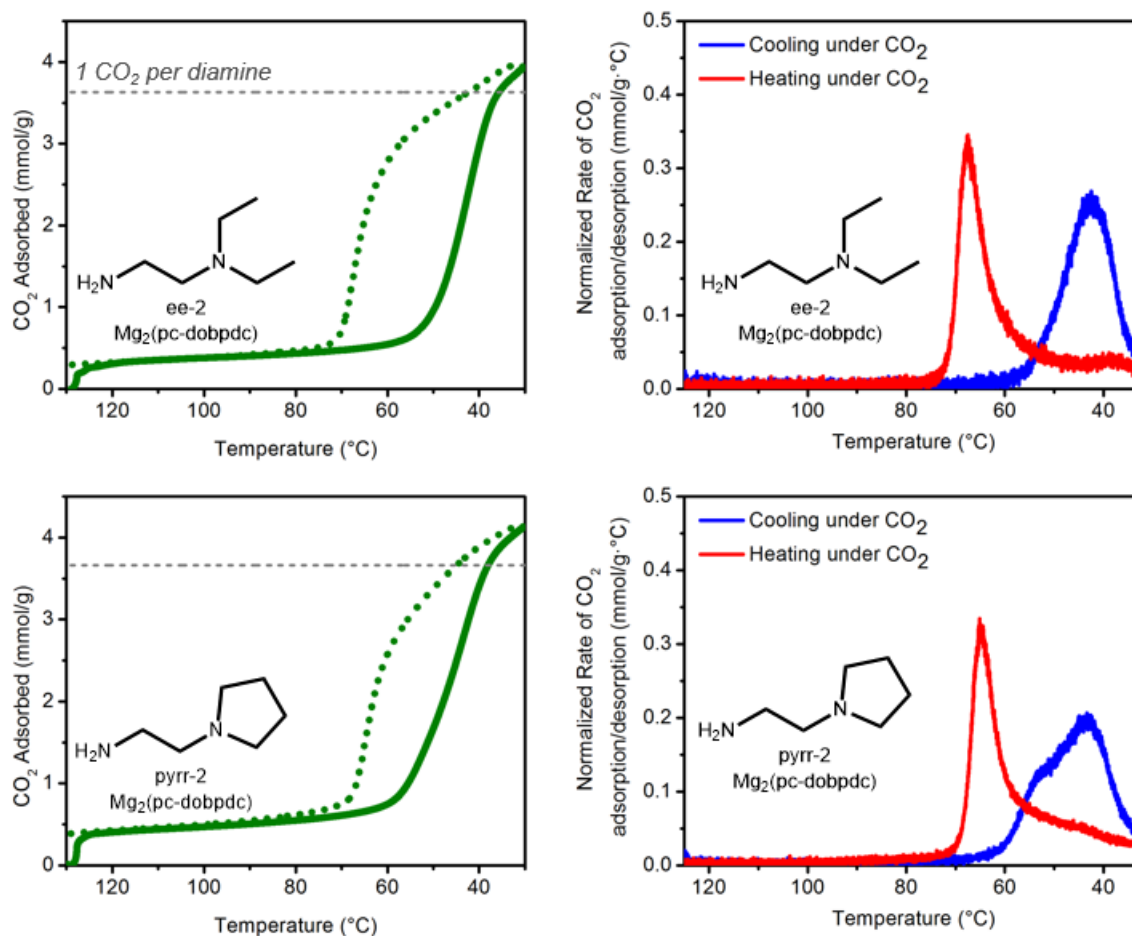


**Figure S51.** Left: CO<sub>2</sub> adsorption (solid line) and desorption (dotted line) isobars of ee-2-Mg<sub>2</sub>(pc-dobpdc) (top) and pyr-2-Mg<sub>2</sub>(pc-dobpdc) (bottom). Right: The derivative plots of these isobars show one CO<sub>2</sub> adsorption (blue) and desorption (red) step. A ramp rate of 2 °C/min was used.

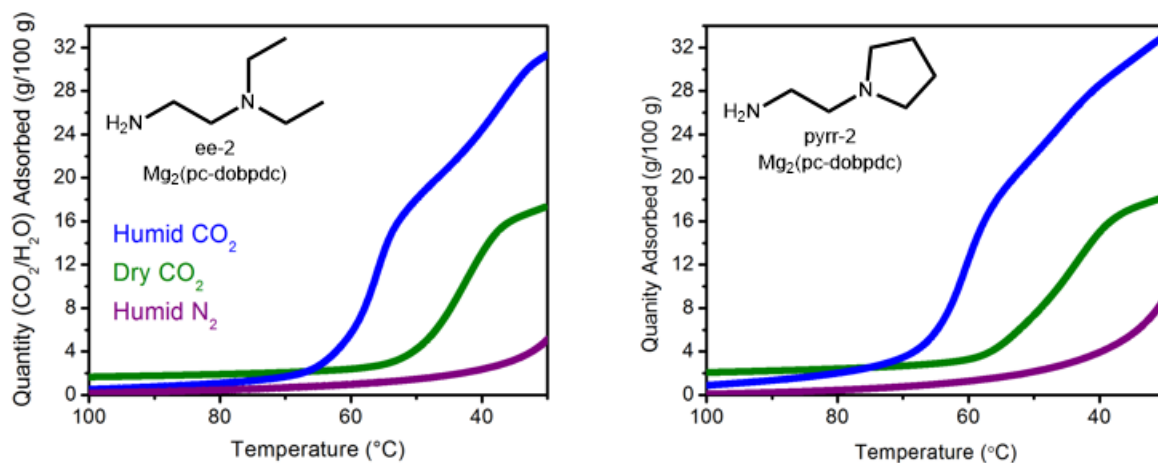


**Figure S52.** Humid N<sub>2</sub> (purple), dry CO<sub>2</sub> (green), and humid CO<sub>2</sub> (blue) adsorption isobars of ee-2-Mg<sub>2</sub>(pc-dobpdc) (left) and pyr-2-Mg<sub>2</sub>(pc-dobpdc) (right). In both cases, the apparent CO<sub>2</sub> adsorption steps are shifted to higher temperatures, accompanied by significant water co-adsorption. The diamine loadings were found to be 99% and 100% after the humid TGA experiments, respectively, as determined by <sup>1</sup>H NMR after digestion with DCl. A ramp rate of 2 °C/min was used.

## 11. Single-crystal X-ray diffraction structure of $\text{Zn}_2(\text{pc-dobpdc})(\text{DMA})_2$ .

Single-crystal X-ray diffraction data for  $\text{Zn}_2(\text{pc-dobpdc})(\text{DMA})_2$  were collected at Beamline 11.3.1 at the Advanced Light Source, Lawrence Berkeley National Laboratory, using synchrotron radiation ( $\lambda = 0.7749 \text{ \AA}$ ) and a Bruker AXS D8 diffractometer equipped with a Bruker PHOTON 100 CMOS detector. The crystal was flash-cooled to 100 K using an Oxford Cryosystems Cryostream 700 Plus. Analysis of the diffraction pattern revealed the crystal to be an obverse/reverse twin, and the program CELL\_NOW<sup>8</sup> was used to determine the orientation matrices. The diffraction pattern was indexed to two domains that were found to be related by a  $180^\circ$  rotation about the reciprocal axis  $[0\ 1\ 1]$ . Raw data for both twin matrices were integrated and corrected for Lorentz and polarization effects using Bruker AXS SAINT<sup>9</sup> software and were corrected for absorption using TWINABS.<sup>10</sup> TWINABS was used to produce a merged HKLF4 file, which was used for initial structure solution and initial refinement, and an HKLF5 file, which was used for the final refinement. The HKLF5 file contained the first component of the merged reflections, and those that overlapped with the second component were split into 2 reflections. TWINABS indicated the twin fraction to be 97:3. The structure was solved using SHELXT<sup>11</sup> and refined using SHELXL<sup>12,13</sup> operated in the OLEX2 interface.<sup>14</sup> Thermal parameters were refined anisotropically for all non-hydrogen atoms. All hydrogen atoms were placed geometrically and refined using a riding model. Unbound solvent molecules within the pores of the framework were highly disordered and could not be modeled. Therefore, the Platon routine SQUEEZE<sup>15</sup> was used following refinement of the complete framework structure model.

**Table S9.** Crystallographic Data

	Zn <sub>2</sub> (pc-dobpdc)(DMA) <sub>2</sub>
Formula	C <sub>22</sub> H <sub>24</sub> N <sub>2</sub> O <sub>8</sub> Zn <sub>2</sub>
Temperature (K)	100(2)
Crystal System	Trigonal
Space Group	$R\bar{3}$
a, b, c (Å)	36.5943(12), 36.5943(12), 6.7186(2)
$\alpha, \beta, \gamma$ (°)	90, 90, 120
V, (Å <sup>3</sup> )	7791.8(6)
Z	9
Radiation, $\lambda$ (Å)	Synchrotron, 0.7749
2 $\Theta$ Range for Data Collection (°)	4.854 to 85.714
Completeness to 2 $\Theta$	99.8% (2 $\Theta$ = 55.412°)
Data / Restraints / Parameters	9707 / 0 / 158
Goodness of Fit on F <sup>2</sup>	1.066
R1 <sup>a</sup> , wR2 <sup>b</sup> (I > 2 $\sigma$ (I))	0.0595, 0.1618
R1 <sup>a</sup> , wR2 <sup>b</sup> (all data)	0.0776, 0.1712
Largest Diff. Peak and Hole (e Å <sup>-3</sup> )	1.777 and -1.440

$$^a R_1 = \sum ||F_o| - |F_c|| / \sum |F_o|. \quad ^b wR_2 = \{ \sum [w(F_o^2 - F_c^2)^2] / \sum [w(F_o^2)^2] \}^{1/2}.$$

## 12. References.

- (1) Lee, J.-W.; Klajn, R. *Chem. Commun.* **2015**, 51, 2036.
- (2) Siegelman, R. L.; McDonald, T. M.; Gonzalez, M. I.; Martell, J. D.; Milner, P. J.; Mason, J. A.; Berger, A. H.; Bhowan, A. S.; Long, J. R. *J. Am. Chem. Soc.* **2017**, 139, 10526.
- (3) Xiao, D. J.; Oktawiec, J.; Milner, P. J.; Long, J. R. *J. Am. Chem. Soc.* **2016**, 138, 14371.
- (4) McDonald, T. M.; Lee, W. R.; Mason, J. A.; Wiers, B. M.; Hong, C. S.; Long, J. R. *J. Am. Chem. Soc.* **2012**, 134, 7056
- (5) Kinzel, T.; Zhang, Y.; Buchwald, S. L. *J. Am. Chem. Soc.* **2010**, 132, 14073.
- (6) Deng, H.; Grunder, S.; Cordova, K. E.; Valente, C.; Furukawa, H.; Hmadeh, M.; Gandara, F.; Whalley, A. C.; Liu, Z.; Asahina, S.; Kazumori, H.; O’Keeffe, M.; Terasaki, O.; Stoddart, J. F.; Yaghi, O. M. *Science* **2012**, 336, 1018.
- (7) McDonald, T. M.; Mason, J. A.; Kong, X.; Bloch, E. D.; Gygi, D.; Dani, A.; Crocellà, V.; Giordanino, F.; Odoh, S. O.; Drisdell, W. S.; Vlasisavljevich, B.; Dzubak, A. L.; Poloni, R.; Schnell, S. K.; Planas, N.; Lee, K.; Pascal, T.; Wan, L. F.; Prendergast, D.; Neaton, J. B.; Smit, B.; Kortright, J. B.; Gagliardi, L.; Bordiga, S.; Reimer, J. A.; Long, J. R. *Nature* **2015**, 519, 303.
- (8) G. M. Sheldrick, *CELL NOW V2008/2*, Bruker AXS Inc, 2008.
- (9) Bruker Analytical X-ray Systems, Inc., *SAINT and APEX 2 Software for CCD Diffractometers*, Bruker Analytical X-ray Systems, Inc., Madison, WI, USA, 2000.
- (10) G. M. Sheldrick, *TWINABS, Version 2012/1*, University of Göttingen, 2012.
- (11) Sheldrick, G. M. *Acta Crystallogr. Sect. Found. Adv.* **2015**, 71, 3.
- (12) G. M. Sheldrick, *Acta Crystallogr., A, Found. Crystallogr.* **2008**, 64, 112.
- (13) G. M. Sheldrick, *SHELXL*, University of Göttingen, Germany, University of Göttingen, Germany, 2014.
- (14) O. V. Dolomanov, L. J. Bourhis, R. J. Gildea, J. A. K. Howard and H. Puschmann, *J. Appl. Crystallogr.* **2009**, 42, 339.
- (15) Spek, A. L. *Acta Cryst.*, **C71**, 9–18.